united nations
educational, scientific
and cultural
organization

international atomic
energy agency

the
**abdus salam**
international centre for theoretical physics

**School on "Exploring the Atmosphere by Remote Sensing Techniques"**
**18 October - 5 November 1999**

**1151-26**

---

# "Inverse Methods in Atmospheric Physics"

**R. Guzzi**
**ISAO/CNR**
**Bologna**
**Italy**

---

*Please note: These are preliminary notes intended for internal distribution only.*

# Inverse Methods in Atmospheric Physics

Rodolfo Guzzi
ISAO Cnr, Bologna Italy

November 1, 1999

# 1 Introduction

**This document is still in the drafting stage. It is released only to give, to the students, an overview on the inversion methods. Beware of the algebra, may contain some errors**

The words inverse methods cover a lot of different branches in geophysics. Such a document wants to cover some aspects of the remote sensing in atmosphere.

First of all one starts from the well known direct methods. They involve the use of physical imitative models that are based on the solution of radiative transfer equation in atmosphere. Its complexity is out of my t lk, but in principle we may say that a model is a combination of different information coming from the optical properties of the atmosphere. So in general a model may contains, for instance, the better solution of the radiative transfer equation of a atmosphere-underlying surface system coupled with the optical properties of the atmospheric components like aerosol and clouds (obtained by Mie theory for spherical atmosphere or by other theory for non-spherical aerosol applied to different classes whose refractive index can be known) toghether with the cross sections of gases. Such a model can be used in the main complex cases ( for instance in the case in which the satellite looks at nadir) to produce complicated algorithm where the radiance measured by the satellite $R_meas$ can be compared to the simulated cases over different scenarios by minimizing the following relation:

$$\chi^2(\mu,\phi,\theta;a_{ref},\tau) = \sum_j \left(\frac{R_{meas}(\mu,\phi,\theta;a_{ref},\tau) - R_{sim}(\mu,\phi,\theta;a_{ref},\tau)}{\sigma}\right)^2 \quad (1)$$

$$j = 1,...N$$

In such a case the minimizing techniques along the satellite viewing geometry $(\mu,\phi,\theta;a_{ref})$ subject to an error $\sigma$ like the Levenberg-Marquardt tecnique or others are massively used to produce the wanted values (surface reflection $a_{ref}$, gas concentration, aerosol and cloud optical thickness $\tau$ and so on). However such a procedures are time consuming and requires fast computer and huge amount of mass storage. On the contrary in case of limb measurements the algorithms are relatively simple and are based on Freedholm equation of the first kind and proper solution that will be the object of such paper.

# 2 Numerical methods

Most inverse problems involve integral transform

$$\int_a^b k_i(x)f(x)dx \tag{2}$$

but numerical calculation for arbitrary $f(x)$ rely on the approximation of this integral by sum known as *quadrature.*

A simple quadrature example involves deviding the interval $(a, b)$ into shorter interval by interposing N quadrature points $x_1, x_2....x_N$ within the interval, envisaging $f(x)$ to take the value $f_1, f_2...f_N$ at those points and to behave linearly across the subintreval $x_j-¿x_{j+1}$. If $f(x)$ takes a fixed values at $x = a$ The quadrature points include $x = a$, $x = b$.

The integral can be approximate by summing over all the subintervals the integral

$$\int_{x_j}^{x_{j+1}} (A_j + B_j x)k_i(x)f(x)dx \tag{3}$$

where $A_j$ and $B_j$ are chosen to make $A_j + B_j x$ coincident with $f(x)$ at $x = x_j$ and $x_{j+1}$.

To accomplish this :

$$A_j + B_j x_j = f_j \tag{4}$$
$$A_j + B_j x_{j+1} = f_{j+1} \tag{5}$$

So that

$$B_j = \frac{f_{j+1} - f_j}{x_{j+1} - x_j} \tag{6}$$
$$A_j = \frac{x_{j+1}f_{j+1} - x_j f_j}{x_{j+1} - x_j} \tag{7}$$

Then the interval $x_j-¿x_{j+1}$ makes the following contribution:

$$A_j \int_{x_j}^{x_{j+1}} k_i(x)f(x)dx + B_j \int_{x_j}^{x_{j+1}} xk_i(x)f(x)dx \tag{8}$$

that can be broken in terms of factor $f_j$ and $f_{j+1}$. Substituting and adding the contribution of all subinterval $x_{j+1}$ and $x_{j+2}$ and so on, one finally obtains the *Quadrature Formula*:

$$\int_a^b k_i(x)f(x)dx \approx \sum_{j=1}^{N} w_j f_j \tag{9}$$

where $w_j$ is given by:

$$\begin{aligned}[\frac{x_{j+1}}{x_{j+1}-x_j}\int_{x_j}^{x_{j+1}} k(x)dx - \frac{1}{x_{j+1}-x_j}\int_{x_j}^{x_{j+1}} xk(x)dx]f_j + \\ +[\frac{-x_j}{x_{j+1}-x_j}\int_{x_j}^{x_{j+1}} k(x)dx + \frac{1}{x_{j+1}-x_j}\int_{x_j}^{x_{j+1}} xk(x)dx]f_{j+1}\end{aligned} \tag{10}$$

The accuracy of the quadrature can improve by increasing the number of points, if $k_i(x)$ change rapidly a very fine subdivision may be neede. The integrals can be evaluate both numerically or analitically. One can select a suitable quadrature formula such as:

$$g(y) = \int_a^b k(y,x)f(x)dx \tag{11}$$

to the linear approximation:

$$\begin{aligned}\mathbf{g} &= \mathbf{Af} \\ (M\text{x}1) &= (M\text{x}N)(N\text{x}1)\end{aligned} \tag{12}$$

where f contains the values of f(x) at the selected representative set of tabular points $x-1, x_2....x_N$ and g contains the m values of g , $g_1, g_2...g_N$. Equation 13 is a system where M and N are often large and the measured nature of g and the finite accuracy of the quadrature formulae alone ensure that there is always a small error component in the linear equation. So when we invert the system we invert not g but $g+\epsilon$ where is an error that can be estimate, but whose sign is not known. Eq. 13 can have the following properties:

1. can be contraddictory ( contradiction in parametrs)
2. do not have enogh information (information not independent)

3. unstable ( det A very small or singular)

4. undetermined (N unknowns > N equations)

5. overdetermined (N unknowns > N equations).

# 3 Analysis error

## 3.1 Measurement error

In such a case the analysis of conditioning (i.e. the evolution of the effects of errors on the vector f obtained by the inversion matrix) is evaluated by means of the amplification of the percentage related to vector g respect to the percentage error related to solution vector.

$$\frac{\|\delta f\|}{\|f\|} = \chi \frac{\|\delta g\|}{\|g\|} \tag{13}$$
$$\chi = \frac{\|\delta f\|}{\|f\|}\frac{\|g\|}{\|\delta g\|} = \frac{\|A^{-1}\delta g\|}{\|A^{-1}g\|}\frac{\|g\|}{\|\delta g\|}$$

that has an upper limit given by:

$$\chi \leq K(A) = \|A\|\|A^{-1}\| \tag{14}$$

$\|X\| = (\sum_{i=1}^{N} |X_i|^2)^{1/2} = \sqrt{X^T X}$ is the norm 2.

## 3.2 Error in determining the matrix coefficients

Are all the errors and uncertainties regarding the physical parameters.

If the matrix A is perturbed by $\delta A$ (that is the error in determining the matrix coefficients), we have:

$$A' = A + \delta A \tag{15}$$

If the matrix is not singular the error amplification is:

$$\chi_c = \frac{\|\delta f\|}{\|f\|} \frac{\|A\|}{\|\delta A\|} \tag{16}$$

and since

$f' = f + f = A(I + A^{-1}\delta A)g = Ag + A^{-1}\delta Ag$ and
$\delta f = A^{-1}\delta Ag$

$$\chi_c = \frac{\|A^{-1}\delta Ag\|}{\|A^{-1}g\|} \frac{\|A\|}{\|\delta A\|} \tag{17}$$

### 3.3 Error quadrature

In remote sensing the errors are only an estimation because one needs to know simultaneously the kernel $k(y, x)$ and f. The accuracy depends on the number of nodes and usually increases with the increasing of them.

## 4 Stability analysis

We analyze now what is the effect that the uncertainties have on the determination of the component of $g(y_j)$ and what are the consequence on retrieval.

Inverting the matrix A and multiplying it by a vector $g + \delta g$ we have

$$f' = A^{-1}(g + \delta g) \neq f \tag{18}$$

If the system is ill-conditioned it produces great instability on solution. In such a case one needs to work on matrix.

### 4.1 least square solution

It consists in finding a vector solution f" such to minimize the norm of vector $Af" - g$. Then:

$$r\|Af" - g\|^2 = (Af" - g)^T(Af" - g) = \tag{19}$$
$$f"^T A^T Af" - g^T Af" - g^T Af" - f"^T A^T g + g^T g$$

Making the derivative of r and putting it equal zero we obtain the minimum. We note that when a vector is differentiated respect to one of its component, the result is a vector with null element everywhere but the kth position where the vector is unitary. Such a versor is $e_k$. Then

$$e_k^T A^T A f" + f"^T A^T A e_k - g^T A e_k - e_k^T A^T g = 0 \qquad k = 1, N \tag{20}$$

or

$$e_k^T (A^T A f" - A^T g) + (f"^T A^T A - g^T A) e_k = 0 \tag{21}$$

noting the first term is transpose of the first we can write

$$(A^T A f" - A^T g) = 0 \tag{22}$$

or

$$f" = (A^T A)^{-1} A^T g = 0 \tag{23}$$

Analizing such a function we see that we cannot obtain a better solution than that obtained using a simple inversion. Infact the $(A^T A)^{-1}$ is greater than $A^{-1}$ since $det(AA^{-1}) = (detA)^2$.

## 4.2 Regularization

On the basis of prevoius results, we need to modify the matrix. But modify the matrix it is to modify the system itself. We introduce a multiplier $\gamma$ such as

$$p(f) = \|Af - g\|^2 + \gamma q(f) \tag{24}$$

where $p(f)$ is a certain function depending on $f$, for instance :

$$q(f) = \sum_{i=1}^{N} (f_{i-1} - f_i)^2 \tag{25}$$

or

$$q(f) = \sum_{i=1}^{N} f_i^2 \tag{26}$$

Such a last equation is called function at "minimum energy" When $\gamma$–¿$\infty$, $q(f) = 0$. In general once $\gamma$ is a priori fixed, f' obtained by minimizing p(f) is such that the difference beetween the vector $g' = Af$ and the vector $g$ is less than the estimated error of measurements.

$$r(f) = \|Af - g\|^2 ¿ |dg| \tag{27}$$

Now we select from the subsets a unique f which is the smoothest as judged by the measured $q(f)$

### 4.2.1 Measure of smoothest

Most measure of non-smmothest are simple quadratic combination of $f_i$ and are therefore forms of $f$ which can be written as:

$$q(f) = fHf \tag{28}$$

where H is a simple near diagonal matrix. If H is a symmetric matrix then:

$$H = K^T K \tag{29}$$

$K$ being such $kf$ contains in its elements that are squared and summed to give $q$; or the quadratic form is the squared norm of the vector $kf$. If we have "minimum energy" $H = I$ where $I$ is the identity matrix.

## 4.3 Completion of constrined solution processes

Now we want to minimize:

$$p(f) = (Af - g)^T(Af - g) + \gamma f^T H f \tag{30}$$

It means to minimize the derivative of the equation 30 in the same way we have already done in previous case. Being the second term the transpose of the first one we put equal zero the first term for each value of k and we obtain:

$$(A^T A + \gamma H)f = A^T g \tag{31}$$

or the known

$$f = (A^T A + \gamma H^{-1})A^T g \tag{32}$$

where the eigenvalues of the $A^T A + \gamma H$ matrix are greater of those of matrix $A^T A$ and the system is stable.

### 4.3.1 Searching the optimal $\gamma$

We have now found a new formulation of the type

$$f = B^{-1} g \tag{33}$$

where

$$B^{-1} = (A^T A + \gamma H^{-1})A^T \tag{34}$$

Since the known vector is g we have obtained a new unknown function that can be equal to previous only if $\gamma = 0$

Putting

$$f' = f + \delta f \tag{35}$$

where $\delta f$ is due to the variance of the matrix itself, we have a new system of the type:

$$f' + df' = B^{-1}(g + dg) \tag{36}$$

with $df'$ is due to the error introduced on g. Then:

$$f' + \delta f + df' = B^{-1}(g + dg) \tag{37}$$

remembering $f = A^{-1}g$ we have

$$\delta f + df' = B^{-1}(g + dg) - A^{-1}g = (A^T A + \gamma H)^{-1} A^T (g + dg) - A^{-1}g \tag{38}$$

The right part represents the total variation of the unknown function due to the modification of the matrix and introducing the error vector g for $\gamma$¿0 and increasing the contribution related to $\delta f$ increases, decreasing for $df'$ producing a better conditioning. The optimal value of $\gamma$ is that minimizes the equation 38. We put then

$$\|\delta f + df'\| = \|B^{-1}(g + dg) - A^{-1}g\| \tag{39}$$

and $\gamma$ such as it is minimum. When $\gamma$ is selected we need to verify if it is acceptable or

$$\begin{aligned} \|Af' - g\| &> \epsilon \\ \|(AB^{-1} - I)g\| &\leq \epsilon \end{aligned} \tag{40}$$

# 5 Information content

The question then arises now is : how many measurements need to have a significant information content?

The first point is to decide how many are the independent measurements. But this is not obvious because we can have a lot of measurements independent but that cannot introduce other information Then we look at the kernel's trend that determines the matrix A, determines the vector f and the error dg. The main problem is due to the kernels that are not function mutually ortogonal. Then the mth kernel can be approximated by a linear combination of other kernels plus an error that can be minimized. Infact from

$$g_m = \int k_m(x) f(x) dx \tag{41}$$

it is evident that the kth kernel is a linear combination of m-1 kernel or

$$k_m(x) = \sum_{j \neq m} a_j k_j(x) \tag{42}$$

and then:

$$g_m = \int \sum_{j \neq} a_j k_j(x) f(x) dx = \sum_{j \neq} a_j \int k_j(x) f(x) dx = \sum_{j \neq m} a_j g_j(x) \tag{43}$$

The kth kernel can be approximated by the previous relation through a relation of the type

$$\int [k_m(x) - \sum_j a_j k(x)]^2 dx \tag{44}$$

where $a_j$ are properly selected.

Then

$$k_m = \sum_j a_j k(x) + \epsilon(x) \tag{45}$$

Or introducing the error $\delta_m$, we have:

$$g_m = \sum_{j \neq m} a_j g_j(x) + \delta_m \tag{46}$$

How small can we make $\sum_j a_j k(y_j, x)$ Observing the absolute magnitude of a's is irrelevant we loose no generality by choosing the constraint: $\sum_j a_j^2 = 1$

Then as measure of the smallest of this quantity the squared norm is appropriate. The problem becomes that of determining the condition for

$$q = \int [\sum_j a_j k(y_j, x)]^2 dx \tag{47}$$

to attain extremum subject to the constraint $\sum_j a_j^2 = a^T a = 1$. If we collect the $k_i(x)$ into a vector $\mathbf{k(x)}$, the scalar quantity $k_j a_j k_j(x)$

is simply $a^T\mathbf{k}(\mathbf{x})$ and the square is $a^T\mathbf{k}(\mathbf{x})k^T(x)a$. But matrix-vector products are associative. So we can write:

$$[a^T\mathbf{k}(\mathbf{x})][k^T(x)a] = a^T[\mathbf{k}(\mathbf{x})k^T(x)]a \tag{48}$$

Only the matrix is a function of x, so the integral 47 can be written as

$$a^T C a \tag{49}$$

where C is the covariance matrix obtained by taking all pairs of kernel and integrating their products over the range of x with which the inversion problem is concern.

Then the information content useful for retrieving f(x) is related with the eigenvalues $\lambda$ of the covariance matrix, previously defined whose elements are $c_{ij} =_i (x)k_j(x)dx$, by the relation

$$\lambda_i \gg \frac{\sum_{j=1}^{N} dg_i^2}{\sum_{j=1}^{N} f_j^2} = (\frac{\|dg\|}{\|f\|})^2 \tag{50}$$

If we consider the relative error as given by

$$RE^2 = (\frac{\|dg\|}{\|g\|})^2 \tag{51}$$

we obtain:

$$\lambda_i \gg RE^2(\frac{\|Af\|}{\|f\|})^2 \tag{52}$$

Since such a relation does not contain the simple symbol > it follows that the method does not give absolute information around the exact number of useful information to make retrieval of f(x) when the eigenvalues are of the same order of the right part of relation 52. However if exist N' eigenvalues less than the treshold given by equation 52 the measurements able to give independent information are N-N'.

Then the relation 52 gives:

(a) the information content associated to the kernel and it is able to evaluate the number of independent information, when the relative error and the guessed f(x) are given

(b) an indication for the optimal $\gamma$ to use during the constrained inversion

(c) the estimation of the relative max error allowable in order to avoid the instability of the solution when one makes the direct inversion $f = A^{-1}g$

# 6 Retrieving the aerosol profile

As an example we can use such methodology based on a Freedholm equation of the first order. We suppose to have solved the Radiative Transfer Equation in such a way to have a relation of the following type:

$$I = \frac{1}{\mu} \sum_{l} \int_0^{\tau_0} \beta_l e^{-q_l \tau} d\tau \tag{53}$$

where the vector $q_l = (k + \frac{1}{\mu}, -k + \frac{1}{\mu}, \frac{1}{\mu_0} + \frac{1}{\mu}, b + \frac{1}{\mu}, -b + \frac{1}{\mu})$ and $l = 1, 2, 3, 4, 5$.

## 6.1 Limits of confidence of the model

Since the solution can be only obtained by an approximated solution where the phase function is truncated, we introduce the following scaled quantities;

$$\begin{aligned} g' &= \frac{g - f}{1 - f} \\ \omega_0' &= \frac{(1 - f)\omega_0}{1 - \omega_0 f} \\ \tau' &= (1 - \omega_0 f)\tau \end{aligned} \tag{54}$$

where $f$ is the fractional scattering of radiation into the forward peak given as the second Legendre polynomial expansion ratio 5. Tests carried out by Xiang at al (1994) showed that for $\tau$¿3 we may use the actual phase function and $\omega_0'$ and $\tau'$

## 6.2 Retrieval method of aerosol profile variations

Taking into account that the optical thickness is :

$$\tau = \int_z^\infty \alpha(\chi) d\chi \tag{55}$$

and

$$d\tau = -\alpha(z) dz \tag{56}$$

the total upward radiance changes as a conseguence of the variation of the aerosol extinction profile $\delta\alpha(z)$ can be written as:

$$\delta I = \frac{1}{\mu} \sum_l \int_0^\infty [\beta_l(z)\delta\alpha(z) e^{-q_l(z)\int_z^\infty \alpha(\chi)d\chi} \tag{57}$$

$$-\beta_l(z)\alpha(z) e^{-q_l(z)\int_z^\infty \alpha(\chi)d\chi} q_l(z) \int_z^\infty \delta\alpha(\chi) d\chi] dz$$

Such equation can be transformed as follows:

$$\delta I = \sum_l \int_0^\infty W_l(\gamma; z)\delta\alpha_A(z) dz \tag{58}$$

where:

$$W_l(\gamma; z) = \frac{1}{\mu}[\beta_l(z) e^{-q_l(z)\int_z^\infty \alpha(\chi)d\chi} \tag{59}$$

$$- \int_0^z \alpha(\chi)\beta_l(\chi) q_l(\chi) e^{-q_l(\chi)\int_\chi^\infty \alpha(t)dt} d\chi]$$

Then the equation (25) is:

$$g(\lambda, \gamma) = \int_0^\infty K(\lambda, \gamma; z) f(z) dz \tag{60}$$

where the relative aerosol variation $f(z) = \frac{\delta\alpha(z)}{\alpha(z)}$ while the aerosol kernel function is given by $K(\lambda, \gamma; z) = \sum_l \alpha(\lambda; z) W_l(\lambda, \gamma; z)$. The quadrature scheme, based on the trapezoidal rule, may be applied to $W_l$. Then we obtain:

$$W_l(i) = \frac{1}{\mu}[\beta_l(i) T(i)^{q_l(i)} - \tag{61}$$

$$\sum_{m=1}^{i-1} \alpha(m)\beta_l(m) q_l(m) T(m)^{q_l(m)} \Delta z^+(m) -$$

$$\alpha(i)\beta_l(i) q_l(i) T(i)^{q_l(i)} \Delta z^-(i)]$$

Where $T(n) = e^{-\int_{z(n)}^{\infty} \alpha(\chi) d\chi}$ is the transmittance from the $z(n)$-layer to TOA. Then the numerical evaluation can be carried out as:

$$g((\lambda,\gamma)_j) = \sum_{i=1}^{N} K((\lambda,\gamma)_j; i) f(i) \Delta z(i) \tag{62}$$

where the index $j$ identifies the wavelenght and scattering angle considered, while N identifies the atmospheric layer. The equivalent matrix form is:

$$\mathbf{g} = \mathbf{A}\mathbf{f} \tag{63}$$

From now on the inversion can be treated by the procedure previously developed i.e.

$$\mathbf{f} = (\mathbf{A}^{\mathbf{T}}\mathbf{A} + \gamma\mathbf{H})^{-1}\mathbf{A}^{\mathbf{T}}(\mathbf{g} + \mathbf{dg}) \tag{64}$$

where the matrix H is the identity matrix and dg is experimental uncertainty in g

# 7 Conclusions

Retrieval from satellite is a complex and difficult task. For this reason many different methods are used from the minimization techniques to inversion method of ill-posed problem. This paper deals with main techniques currently used.

# 8 Bibliography

[2] M. Gabella, R. Guzzi, V. Kissilev and G. Perona, " Retrieval of aerosol profile variations in the visible and near infrared; theory and application of the single scattering approach" Applied Optics, 1997, pp 1328-1336

[3] V.V. Sobolev, " Light scattering in planetary atmospheres", Pergamon Press, 1975

[4] X. Xiang, E.A. Smith, C. G. Justus, "A rapid radiative transfer model for reflection of solar radiation" J.A.S. vol 51, N0 13 pp 1978-1988, 1994

# The application of the Radiative Transfer Theory to the information content modelling connected with the interpretation of a multispectral satellite environment data

Rodolfo Guzzi [1], Oleg Smokty [2]
IMGA-CNR, via Emilia Est 770, Modena (Italy)
[2] Institute for Informatics and Automation, Russian Academy of Science, 14 line 39, San Petersburg (Russia)

## 1 Abstract

The information content of the optical atmospheric data retrieved, making use of multispectral satellite measurements in the visible and near infrared spectral regions is modelled by direct and inverse radiative models based on a unified mathematical description. The semantic kernel of such approach consists in the unifying the mathematical modelling that contains from one side the direct-inverse operator and the inputs optical models of the atmosphere-surface system.

The appropriate numerical results for forward input optical and direct radiative models are here discussed too.

## 2 Introduction

It is well known that modern remote sensing investigations of the environment have to be based on the whole information content determined by the complexity of the experimental and theoretical tools including the receiving system and thematic data analysis. In such context, due to the high cost of receiving and processing data, the appropriate mathematical modelling based on imitative models, assume great significance.

Unfortunately, at present, we have only fragmentary approaches and methods that should be unified to form the appropriate knowledge data system to have the estimation, control, prediction and management of the geophysical and biophysical parameters and processes.

Naturally the total realization of such approach shall be possible only in future. In the present paper, however, we can give some results that illustrate the possibilities of complex imitative mathematical approach based on proper Input Optical Models (IOM) and Forward Radiative Transfer Models (FRTM).

We have selected as proper input optical models that one developed in RADCOM ([1]), and properly related with that one prepared for the Global Ozone Monitoring Experiment ([2],[3])

## 3 Information content modelling related to the radiation transfer problems

In order to provide the information modelling content, Input Optical Multilayer Models ( IOMM) of the Earth's atmosphere-surface system have to be combined with Radiative Transfer Forward Models (RTFM) adopting analytical, semianalytical and numerical solutions of Radiative Transfer Equation (RTE).

If we represent the RTFM in terms of precise and approximate operators L and $\tilde{L}$ respectively and the multitudes of IOMM by exact and approximated parameters G as well as $\tilde{G}$ respectively, we have the following combination:

$$\{L[G] \bigoplus L[\tilde{G}]\} \bigoplus \{\tilde{L}[G] \bigoplus \tilde{L}[\tilde{G}]\}$$

that can be directly apply to the multitudes of unknown intensities $\{I\}_{L,\tilde{L}}$.

The information content of input optical atmosphere-surface system will be determined by a selected discretization level $N[G \bigoplus \tilde{G}]$ and by the appropriate error $\epsilon_N$ that, together represent G and $\tilde{G}$ in each point of the adopted grid g. Then the information content of direct radiative problem will be determined by:

$$\hat{N}\{G \bigoplus \tilde{G}\}, \hat{\epsilon}\{L \bigoplus \tilde{L}] \bigotimes [G \bigoplus \tilde{G}]\}$$

## 4 Atmosphere surface system input optical models

As mentioned before the multitude G contains the input optical information about the spectral optical thickness $\tau_0(\lambda)$, the spectral single scattering albedo $\Lambda(\tau, \lambda)$ and the spectral atmospheric and surface phase function $\chi(\lambda, \gamma, \tau)$.

Then the information content of the input optical models will be defined by:

1. the chosen grid-point g related to the current scattering angle $\gamma$ as a function of solar zenith angle $arcos\zeta$ and observation angle $arcos\eta$ and azimuth angle $\phi$;
2. the spectral wavelenghts discretization $\lambda$;
3. the atmospheric optical thickness $\tau_0(\lambda)$ and optical depth $\tau(\lambda)$;

4. the error level $\epsilon$ of optical parameters representation in each current point of used grid point g.

The next level of information content is determined, according to the classical approach ([4]) by the Fourier transforms taking into account the grid point g and the level of error $\epsilon_N$ including the number of moments $P^m_{atm}(\lambda;\tau,\eta,\zeta)$ and $P^m_{sur}(\lambda;\tau,\eta,\zeta)$ related to the atmospheric and surface phase function $\chi_{atm}(\lambda;\gamma,\tau)$ and $\chi_{sur}(\lambda;\gamma,\tau)$ respectively.

The final level of information content is determined by the summation and successive compression processes of the structurized elements $P^m_{atm,sur}$ provided appropriate calibration procedures.

According to the Nyquist-Kotelnikov's theorem ([5]) the current frequency discretization level k cannot be arbitrary but must exceed twice the highest signal frequency M, i.e.: $k \geq 2M$.

As a result of such approach, taking into account for instance the desiderable level of error equal to $\epsilon = 10^{-4}$ in Table 1 are shown the tabulation scattering angle with the related steps $\Delta\gamma$ needed for the interpolation input atmospheric phase functions.

Table1.
Interpolation scattering angle steps $\Delta\gamma$.
Error is $\epsilon = 10^{-4}$

| $\gamma$ | 0 | 1 | 2 | 3 | 5 | 10 | 15 | 20 |
|---|---|---|---|---|---|---|---|---|
| $\Delta\gamma$ | 0.22 | 0.14 | 1.0 | 0.85 | 0.73 | 0.84 | 1.1 | 1.4 |

| $\gamma$ | 30 | 45 | 60 | 90 |
|---|---|---|---|---|
| $\Delta\gamma$ | 2.0 | 3.0 | 4.2 | 7.4 |

In fig 1 are reproduced the appropriate data related to total number of azimuth harmonics $N_\phi$ (high frequency level) as a function of the logarithm of the error $\epsilon_N$ in terms of the real phase function and Heney-Greenstein parameter g.

# 5 The inverse solution problem related to the Radiative Transfer Theory

The same approach used before can be adopted for the inverse solution. In order to evaluate the moltitudes of $G^*$ and $\tilde{G}^*$ we use the appropriate inverse operators $L^{-1}$ and $\tilde{L}^{-1}$. Then:

$$G^* = \{L^{-1}\{L[G]\} \bigoplus L^{-1}\{L[\tilde{G}]\}\} \bigoplus$$
$$\tilde{G}^* = \{\tilde{L}^{-1}\{\tilde{L}[\tilde{G}]\} \bigoplus \tilde{L}^{-1}\{\tilde{L}[G]\}\}$$

On the basis of discretization level and appropriate error, the information content of inverse problem is:

$$\tilde{M}\{G^* \bigoplus \tilde{G}^*\}, \delta\{L^{-1} \bigotimes [L[G] \bigoplus L[\tilde{G}]] \bigoplus$$
$$\tilde{L}^{-1} \bigotimes [\tilde{L}[\tilde{G}] \bigoplus \tilde{L}[G]]\}$$

The solution of inverse problems of space based atmospheric optics can be given by a unified mathematical approach. Such an approach can be found by the Ambarsumyan's representation for vertical uniform atmosphere bounded from a lambertian reflecting underlying surface ([6]).

By the definition of brightness coefficients $\rho(\eta,\zeta,\phi,\tau_0)$ with surface albedo A, the intensities at the top of the atmosphere $I(0,\eta,\zeta,\phi)$ are:

$$I(0,\eta,\zeta,\phi) = S\zeta\rho(\eta,\zeta,\phi,\tau_0) +$$
$$(A\mu(\eta,\tau_0)\mu(\zeta,\tau_0))/(1 - AC(\tau_0))$$

where $\mu(\zeta,\tau_0)$ and $C(\tau_0)$ are well known parameters defined in Sobolev ([?]) and $\pi S$ is the extraterrestrial irradiance. Brightness coefficient is :

$$\rho(\eta,\zeta,\phi,\tau_0) = \rho^0(\eta,\zeta,\phi,\tau_0) + 2\sum_{i=m}^{M} \rho^m(\eta,\zeta,\phi,\tau_0)cosm\phi$$

$\rho^m(\eta,\zeta,\phi,\tau_0)$ is expressed by the well known Ambarsumyan's functions.

Assuming the space-derived coefficient $\rho(\eta,\zeta,\phi,tau_0)$ is modelled as a result of the direct problem of the radiation transfer theory using similarity ratios for the model phase function containing a certain number of Legendre polynomyals, the inverse problem can be thought on the basis of a spatial angle method.

If we define the set of parameters characterizing the state of environment as $X(x_i)$ and $Y(y_i)$ the spectral brightness measured from space can be written by the following relation:

$Y = AX(x_i)$ with i=1,2,3...n

This relation can be inverted obtaining:

$X(x_i) = A^{-1}Y$ where the inverse operator is incorrect according Hadamard: i.e. small errors in measurements, approximate mathematical form of Y and X and so on. As a consequence the quality of space information must be determined on the basis of following factors:

1.physically based experimental methods of remote sensing and small errors of measured spectral measurements;

2. requirements of mathematically corrected methods and algorithms of environmental parametrs retrieval according to the Earth's brightness spectral measurements data.

Further possibilities consist in a priori parameterization, angular discretization and the use of the analytical form to represent the dependencies of measured radiation field from the unknown state of parameters.

On this basis, an angle discretization method can be applied by the small deviations of retrieved optical parameters values $\delta\tilde{X}_i$ corresponding to small deviation of variaties of retrieved radiation fields $\delta\tilde{Y}_j$ relatively to the varieties of its input values $\delta Y_j$.

Following the scheme of paragraph 3 we have:

$$X_i => X_i + \delta X_i \qquad Y_i => Y_i + Y_i$$
$$i = 1,2,3....N \qquad j = 1,2,3...M$$
$$\Delta\tilde{Y}_j = \delta\tilde{Y}_j + \delta Y_j \qquad \Delta\tilde{X}_i = \delta\tilde{X}_i + \delta X_i$$

Then the following minimization condition has to be fulfilled:

$$\sum_{i,j=1}^{N} |\delta Y(x_j) - \delta\tilde{Y}(x_i)|^2 < \epsilon$$

$$\sum_{i,j=1}^{N} |\delta X_j - \delta\tilde{X}_i|^2 < \delta_\epsilon$$

As an example in figure 2 is presented the errors in retrieving the values of $\tilde{X}_i$ as a function of N.

# 6 Discussion of results and conclusion

On the basis of the approach here presented is evident that dealing with the information content modelling connected with satellite environment data is a complex problem. The approach here outlined is based on a unified mathematical theory starting from the input optical model and using direct and inverse operators to retrieve the optical parameters.

The problem to develop a global environment monitoring from space raises from measuring methods adopted and from the registration and data processing in terms of time-space scale.Such approach requires the formulation of scientifically based requirements for the error and level of discretization as far as we have here briefly presented.

# References


[1] O.Smokty, N.Kobiakov, "Advanced optical aerosol model for the environment forward radiation field computation", IMGA-CNR Tech Rep No4-95, April 95

[2] R.Guzzi,R.Rizzi,G.Zibordi," Atmospheric correction of data measured by a flying platform over the sea: elements of a model and its experimental validation", Applied Optics,pp3043-3051, 1987

[3] R.Guzzi,I.Canossi,M.Cervino,F.Torricella,"High resolution analytical forward model to be applied to high resolution sensors working in the UV and near IR mounted aboard satellite: PIERS 1994 11-16 July Noordwijk pp 2260-2265

[4] V.V.Sobolev"Light Scattering in Planetary Atmospheres" Pergamon Press 1975 Oxford 217pp

[5] O.Smokty,"Modelling of radiation field in the problem of space spectrometry", Pub. Co. Nauka (in Russian) Leningrad,1986,352pp

[6] K.Ya. Kondratiev, V.V. Kozoderov, O.Smokty " Remote Sensing of the Earth from Space: Atmospheric Correction" 1992 Springer-Verlag Berlin 478pp


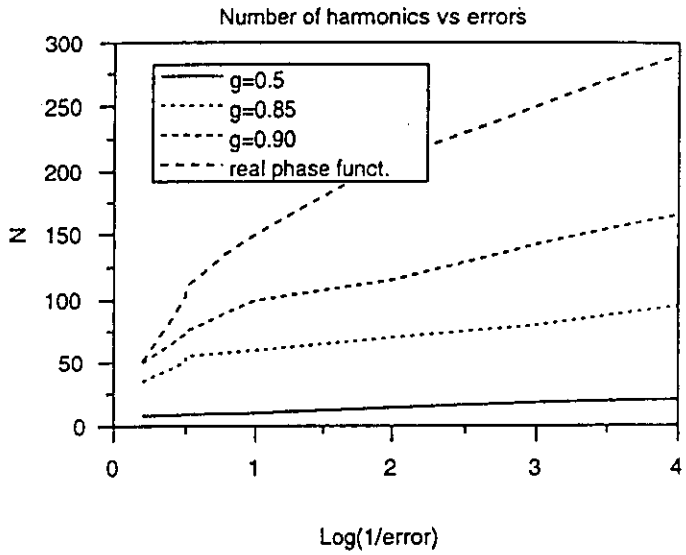


Fig1. Logarithm of the inverse of the errors as a function of Number of harmonics N

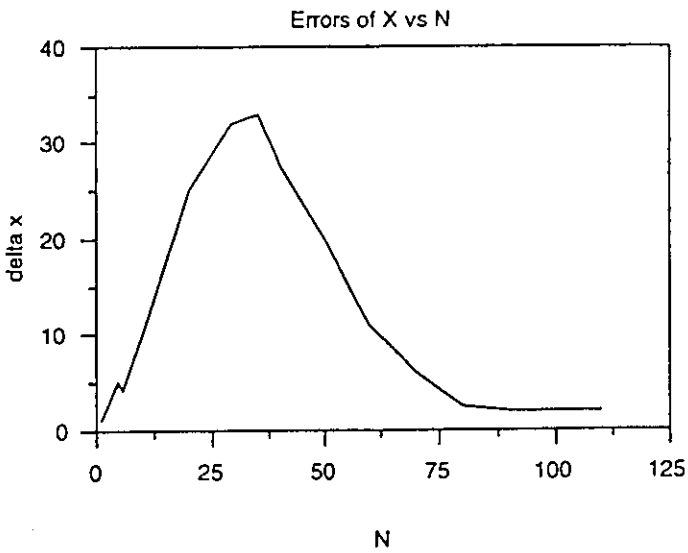


Fig 2. Errors of the retrieving values delta x $=\delta X_i$ in % as a function of N

# Atmospheric aerosol optical properties: a database of radiative characteristics for different components and classes

Chiara Levoni, Marco Cervino, Rodolfo Guzzi, and Francesca Torricella

A database management system has been realized that, by taking physical and chemical properties (the complex refractive index and the size distribution) of basic components as its starting point, allows the user to obtain optical properties of default as well as user-defined aerosol classes. Default classes are defined in accordance with the most widely known and used aerosol models. We obtain user-defined classes by varying the mixing ratio of components, creating new mixtures of default components, or by defining user components, thereby supplying the size distribution and the refractive index. The effect of relative humidity (RH) on the refractive index and the size distribution is properly accounted for up to RH = 99%. The two known mechanisms of obtaining classes from components are allowed (internal or external mixing). © 1997 Optical Society of America

*Key words:* Aerosol optical properties, aerosol models, radiative transfer.

## 1. Introduction

Aerosols play an important role in the global climate, the radiative forcing of climate, and the Earth's radiative balance.

They act by modifying the local and planetary albedo and by absorbing the upward terrestrial thermal radiation. Aerosols influence the radiation balance through two key processes: directly, by scattering and absorbing solar radiation, and indirectly, by acting as cloud condensation nuclei and thus dramatically affecting the optical properties of clouds (the latter is also referred to as the Twomey effect[1]).

The optical properties describing the interaction between aerosol and solar radiation are the extinction ($K^{ext}$) and scattering ($K^{sca}$) coefficients, the single-scattering phase function [$P(\gamma)$], and the vertical optical depth ($\tau_A$): These properties are wavelength dependent and must be specified over the whole spectrum. They are derived from microphysical quantities such as the complex refractive index ($m = n - ik$) and the size distribution [$dN(r)/dr$] by means of the Mie theory, which assumes that the particles are spherical and homogeneous.

Aerosol models represent a simple, generalized description of typical atmospheric conditions.[2] The definition of a model is a complex process because of the great variability in the physical, chemical, and optical properties of aerosols in both time and space. Two fundamental approaches toward defining an aerosol model exist: first, a direct measurement of all the necessary optical properties as a function of space and time and, second, a computation of the optical characteristics of aerosols after the microphysical properties have been collected and averaged by use of data derived from different sources.

The first approach is the most direct. However, it requires a large number of accurate optical measurements for many wavelengths over a representative time period and with adequate spatial coverage. These measurements are currently not available in the required quantity and quality.

For these reasons "computations remain . . . the only reasonable approach to a complete data set of aerosol optical properties needed for a global modelling of climate."[3] Direct optical measurements, when they are available, can subsequently be used for comparison with the computed properties.

Several authors have developed models for atmospheric aerosols: beginning with the early works of Toon and Pollack[4] and Fenn,[5] a number of compila-

The authors are with the Istituto per lo studio delle Metodologie Geofisiche Ambientali, Consiglio Nazionale delle Ricerche, Via Piero Gobetti 101, I-40129 Bologna, Italy.

Received 17 July 1996; revised manuscript received 18 November 1996.

0003-6935/97/308031-11$10.00/0

© 1997 Optical Society of America

tions of aerosol optical properties can be found in the literature,[2,3,6,7] although the great variability of sources and the use of various formats and nonstandardized units make it difficult to use the data.

The Database (in this paper, our Database is denoted by the capital D) provides a powerful tool for obtaining optical properties of default components and aerosol classes. We selected the default components and classes after a thorough analysis of existing published databases by carefully comparing the sources with the aim of drawing up an exhaustive compilation that avoids misleading duplications and adopting a widely recognized nomenclature. The components are defined on the basis of the chemical composition (complex refractive index) and the size distribution. For each component all the relevant microphysical quantities are clearly listed, including the size-distribution type, the wavelength-dependent refractive index, and the information on the ambient humidity dependence of both. The default classes are defined by means of mixing ratios, and they represent typical atmospheric mixtures of standard components. All the default classes are considered as external mixtures. The resulting optical properties of default classes have been checked against published results and measured data (see Section 3).

The main novelty of the Database, besides these default components and classes, is that it allows computation of optical properties of user-defined components and classes. New components are defined by the input of the appropriate refractive index and the size distribution; new classes are achievable by varying the mixing ratios of the default classes or mixing (internally or externally) new components. This flexibility is regarded as a strong improvement with respect to existing databases, and it should meet the need of those scientists who, having analyzed the appropriate standard components or classes to model atmospheric optical properties, are often forced to modify, to a greater or lesser extent, the aerosol characteristic adopted so that it complies with reality.[8–10]

For both default and user-defined classes or components, the optical properties' output is computed on the basis of the user-selected relative humidity (RH) level. The optical properties (extinction coefficient, phase function, single-scattering albedo, asymmetry factor) of the selected class are computed at a set of wavelengths and at a set of angles (phase function) selected by the user.

With the Database it is possible to select the mixing type (internal or external) of components: Indeed, resulting optical properties can vary with the choice of internal or external mixing, thus affecting radiative transfer computations.[11] This capability of the Database to mix the components internally is an important step forward with respect to other available databases in which the components are only externally mixed. Examples of the effect of choosing different mixing types are shown in Section 4.

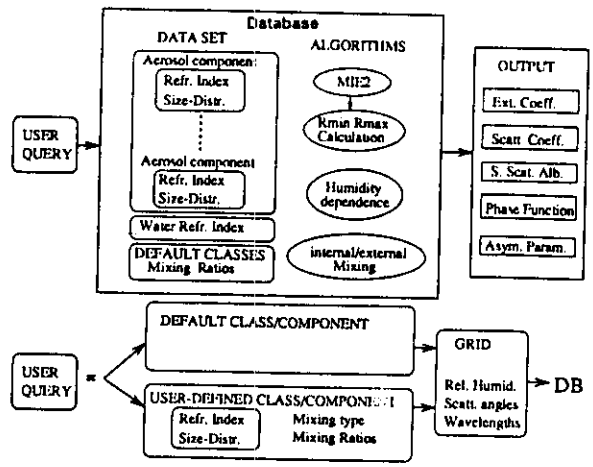


Fig. 1. Database structure, with input–output details.

## 2. Database Structure

### A. Overview

The Database structure is outlined in Fig. 1.

The Database provides defined aerosol class or component optical properties such as extinction, scattering, and absorption coefficients at default concentration (1 particle/cm$^3$), together with phase function, asymmetry parameter, and single-scattering albedo.

An aerosol class is defined as a mixture of aerosol components by the assessment of mixing ratios and mixing type (for an internal or external mixture). Users can select a default aerosol class or component or they can input a user-defined aerosol class or component by setting mixing ratios, size distribution, refractive indices of aerosol components, and mixing type. The difference in mixing type is described in Subsection 2.C. The case of a single-component aerosol class (no mixing) is also allowed.

The user can choose a grid within the following parameter ranges: wavelength, 0.2–40 μm; scattering angle, 0°–180°; and RH, 0%–99%.

The Database algorithms are based on Mie calculations, because aerosol particles are expected to have a spherical shape, which is a reasonable assumption under high humidity conditions, and because most particles are partially composed of hygroscopic material.[6] The sphericity assumption becomes critical as the dry aerosol size increases. Although methods are becoming available to treat shape effects,[12] it was decided to limit the Database computation to the sphericity assumption.

As shown in Fig. 1, the Database consists of a data set of aerosol default components and classes and of some computational algorithms that are presented below.

### B. Data-Set Description

Aerosol components are modeled in the data set by means of continuous distribution functions of the radius (size distributions) due to the sphericity assumption and spectral complex refractive indices. Size

Table 1. Relevant Information on Aerosol Component Size Distributions and Refractive Indices[a]

| Component | dN/dr Type | dN/dr Reference | Wet-Mode Radius | Refractive Indices Type | Refractive Indices Reference |
|---|---|---|---|---|---|
| Dustlike 1 | Log $N$ | 6 | Indep. | Dustlike | 7 |
| Dustlike 2 | Log $N$ | 7 | $n$ | Dustlike | 7 |
| Water soluble 1 | Log $N$ | 6 | 3 | Water soluble | 7 |
| Water soluble 2 | Log $N$ | 7 | $n$ | Water soluble | 7 |
| Soot | Log $N$ | 6 | 3 | Soot | 7 |
| Oceanic | Log $N$ | 7 | $n$ | Oceanic | 7 |
| Sea salt (nuclear) | Log $N$ | 3 | 3 | Oceanic | 7 |
| Sea salt (acc.) | | | | | |
| Sea salt (coarse) | | | | | |
| Mineral background (nucl)[b] | Log $N$ | 3 | Indep. | Mineral | 3 |
| Mineral background (acc)[b] | | | | | |
| Mineral background (coarse) | | | | | |
| Mineral wind carry (nucl)[b] | Log $N$ | 3 | Indep. | Mineral | 3 |
| Mineral wind carry (acc)[b] | | | | | |
| Mineral wind carry (coarse) | | | | | |
| Sulfate | Log $N$ | 3 | 3 | $H_2SO_4$ | 7 |
| 75% $H_2SO_4$ 1 | Log $N$ | 6 | Indep. | $H_2SO_4$ | 7 |
| 75% $H_2SO_4$ 2 | $\gamma$ mod | 7 | Indep. | $H_2SO_4$ | 7 |
| Volcanic ash 1 | Log $N$ | 6 | Indep. | Volcanic ash | 7 |
| Volcanic ash 2 | $\gamma$ mod | 7 | Indep. | Volcanic ash | 7 |
| Mineral long range | Log $N$ | 3 | Indep. | Mineral | 3 |
| Transport to maritime environment | | | | | |
| Mineral Polewards | Log $N$ | 3 | Indep. | Mineral | 3 |
| Small rural | Log $N$ | 2 | 2 | Rural | 2 |
| Large rural | Log $N$ | 2 | 2 | Rural | 2 |
| Small urban | Log $N$ | 2 | 2 | Urban | 2 |
| Large urban | Log $N$ | 2 | 2 | Urban | 2 |
| Maritime-oceanic origin | Log $N$ | 2 | 2 | Oceanic[c] | 2 |

[a]Entries in the third and the fourth columns refer to the publications listed at the end of this paper from which the values of size-distribution parameters and wet-mode radii can be obtained. The label regarding the wet-mode radius is set to $n$ if data are not available, while indep. means that the aerosol component is not hygroscopic. Refractive-index types refer to chemical composition as reported in the cited sources (last column).

[b]The nucl and acc are, respectively, nucleation and accumulation modes.

[c]Values from Shettle and Fenn,[2] which are different from those applied to oceanic and sea-salt components.

distributions are either log-normal or modified gamma distributions:

$$\frac{dN}{dr} = \frac{C}{r \ln(10)\sigma\sqrt{2\pi}} \exp\left\{-\frac{[\log(r/r_m)]^2}{2(\sigma)^2}\right\}, \quad (1)$$

where $r_m$ and $\sigma$ are the mode radius and standard deviation, respectively, and $C$ denotes the default concentration (if the mode radius is expressed in micrometers, $dN/dr$ results in particles per (micrometers times cubic centimeters):

$$\frac{dN}{dr} = Ar^{\alpha} \exp(-br^{\gamma}), \quad (2)$$

where $A$ again denotes the default concentration and $\alpha$, $b$, and $\gamma$ determine the shape of the distribution.

This data set has been collected from several sources, as shown in Table 1. Humidity effects on aerosol-component microphysical properties are taken into account, as suggested by Shettle and Fenn[2] and d'Almeida *et al.*[3] by averaging aerosol and water refractive indices and by changing the mode radius of log-normal size distributions (the standard deviation remains unaffected).

Database components derived by Shettle and Fenn[2] (lower part of Table 1, which begins with the small rural component) have to be considered separately, as they consist of premixed substances with volume-averaged refractive indices. For example, small and large rural components are both composed of 70% water-soluble and 30% dustlike substances, but they obviously differ in size distributions. We decided to include these tropospheric aerosol models to allow users to reproduce those classes (which are labeled SF, for Shettle and Fenn,[2] in Table 2) that represent the basis of the LOWTRAN aerosol database.[13]

Dry aerosol refractive-index values have been collected[7] in the 0.2–40.0-μm wavelength range, except those for mineral components[3] that have been provided in the 0.3–40.0-μm range. Data for Shettle and Fenn aerosol models come from Ref. 2, for the above-mentioned reason. Table 1 shows which of the ten refractive-index types are attributed to each of the 27 components.

By mixing these components it is possible to generate default aerosol classes, presented here in Ta-

Table 2. Default Aerosol Classes[a]

| Aerosol Class | Reference | Aerosol Component | Mixing Ratio |
|---|---|---|---|
| Clean continental | 3 | Water soluble 1 | 0.9999 |
| | | Dustlike 1 | 1.0 $\times 10^{-4}$ |
| Average continental | 3 | Water soluble 1 | 0.93877 |
| | | Dustlike 1 | 2.27 $\times 10^{-6}$ |
| | | Soot | 0.06123 |
| Urban | 3 | Water soluble 1 | 0.5945 |
| | | Dustlike 1 | 1.67 $\times 10^{-7}$ |
| | | Soot | 0.4055 |
| Clean maritime | 3 | Sea salt (nuclear) | 0.512–0.667 |
| | | Sea salt (acc.) | 0.0042–0.03 |
| | | Sea salt (coarse) | 0.001 |
| | | Sulfate | 0.290–0.457 |
| Maritime polluted | 3 | Water soluble 1 | 0.5939 |
| | | Soot | 0.4051 |
| | | Oceanic | 9.6 $\times 10^{-4}$ |
| Desert background (wintertime) | 3 | Mineral background (nucl)[b] | 0.9274 |
| | | Mineral background (acc)[b] | 0.07246 |
| | | Mineral background (coarse) | 0.9661 $\times 10^{-4}$ |
| Desert wind carry (summertime) | 3 | Mineral wind carry (nucl)[b] | 0.8542 |
| | | Mineral wind carry (acc)[b] | 0.14568 |
| | | Mineral wind carry (coarse) | 7.2842 $\times 10^{-6}$ |
| Background stratospheric 1 | 6 | 75% $H_2SO_4$ 1 | 1.0 |
| Volcanic 1 | 6 | Volcanic ash 1 | 1.0 |
| Maritime | 7 | Water soluble 2 | 0.99958 |
| | | Oceanic | 0.00042 |
| Continental | 7 | Water soluble 2 | 0.93876 |
| | | Dustlike 2 | 2.27 $\times 10^{-6}$ |
| | | Soot | 0.06123 |
| Urban or industrial | 7 | Water soluble 2 | 0.5945 |
| | | Dustlike 2 | 1.66 $\times 10^{-7}$ |
| | | Soot | 0.4055 |
| Background stratospheric 2 | 7 | 75% $H_2SO_4$ 2 | 1.0 |
| Volcanic 2 | 7 | Volcanic ash 2 | 1.0 |
| Rural SF | 2 | Small rural | 0.999875 |
| | | Large rural | 0.000125 |
| Urban SF | 2 | Small urban | 0.999875 |
| | | Large urban | 0.000125 |
| Maritime SF | 2 | Small rural | 0.99 |
| | | Maritime-oceanic origin | 0.01 |
| Tropospheric SF | 2 | Small rural | 1.0 |

[a]Data sources, components, and number density mixing ratios for default classes are specified. Entries in the second column refer to the publications listed in the references at the end of this paper.
[b]The nucl and acc are, respectively, nucleation and accumulation modes.

ble 2. The reliability of default classes is discussed in depth in each of the cited source papers. Most of the authors referred to stated that snapshots obtained in a specific location and at a specific time may not conform to the data presented because of averaging processes. Moreover, for marine aerosol types, the default mixing ratios are only estimates because of the high variability of the marine boundary layer; marine default classes have been proposed with the same mixing ratios as those found in the literature.

Finally, it should be noted that mineral long-range transport to a maritime environment and mineral poleward aerosol components in Table 1 are not referred to as part of the aerosol classes in Table 2. As stated in the literature, they form aerosol classes with mixing ratios so variable in time and space that to define default values would not be worthwhile.

### C. Algorithms

#### 1. *Relative Humidity*

With increasing RH values, atmospheric water vapor condenses onto the particles and alters their size and refractive index. This may be applied to hygroscopic particles such as water-soluble or sea-salt components, but makes no sense for insoluble particles such as all mineral components that form desert aerosol classes. The algorithm used for humidity influences on the refractive indices for both real and imaginary parts (the wavelength dependence has been omitted for brevity) is[14]

$$m' = m_w + (m_0 - m_w)(r_0/r')^3, \quad (3)$$

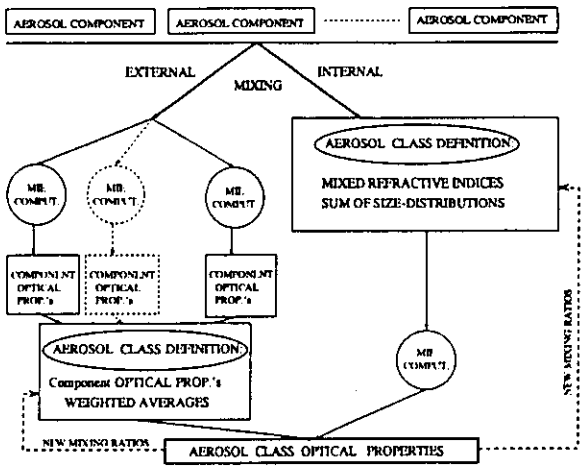


Fig. 2. Internal and external mixing logic flows.

where $m_0$ and $m'$ are the complex refractive indices of dry and wet particles, respectively, $r_0$ and $r'$ are their mode radii, and $m_w$ is the refractive index of water.

The opportunity to use the latter correction suggested by Hänel[15] concerning the imaginary part of the complex refractive index has been provided:

$$\frac{k'}{n'^2+2}=\frac{k_w}{n_w^2+2}+\left(\frac{k_0}{n_0^2+2}-\frac{k_w}{n_w^2+2}\right)\left(\frac{r_0}{r'}\right)^3, \quad (4)$$

where $k$ is the imaginary and $n$ is the real part of the complex refractive index; the prime superscript refers to wet particles, and the 0 and $w$ subscripts refer to dry particles and water, respectively.

### 2. *Mixing Types*

Users have the opportunity to mix the components internally or externally.

In an internal mixture, the individual particle consists of mixed components, whereas in the external mixture, pure particles of various chemical compounds exist side by side. It is currently thought that aerosols often exist initially as external mixtures near aerosol sources and that the aerosols gradually tend toward an internal mixture as they age.

Figure 2 shows the procedure by which the two different types of mixture can be obtained from the same input.

Note that the two procedures lead to distinct results only if aerosol components do not show the same refractive indices. Such refractive-index differences may be due to diverse chemical composition, for example, a clean continental mixture, or to the influence of humidity, as described in Eq. (3) (e.g., rural SF). For example, the distinction between internal and external mixtures cannot be applied to desert aerosol classes, whose nonhygroscopic components differ for size-distribution parameters only.

An internal mixture is characterized by airborne particles with a heterogeneous chemical composition: In view of the difficulty of specifying the refractive index of internal mixtures, aerosol models usually deal only with external mixtures.[6,7] Here the approach adopted is to compute the refractive index of an internally mixed class by use of the volume-weighted average of refractive indices of the components. The computation of volume mixing ratios is derived from number-density mixing ratios and size distributions (see Appendix A). A Mie calculation for internal mixing is then performed just once for each mixture by use of the normalized (by relative particle number densities) sum of size distributions, but requires a new Mie computation every time the particle number-density mixing ratios change.

External mixing implies that each component of a given aerosol class is represented by a different substance with its own size distribution and complex refractive index. Following separate Mie calculations on each component, the resultant extinction (scattering, absorption) coefficient and the other optical properties of the class are obtained as appropriate weighted averages (see Appendix A) by use of concentration by particle number (normalized to 1 particle/cm$^3$).

### 3. *Mie Calculation*

The U.S. Air Force Geophysical Laboratory code used to perform the Mie calculation is MIE2, which is based on a program developed by Radiation Research Associated, Fort Worth, Texas.

The original code required lower and upper integration limits ($r_{min}$ and $r_{max}$, respectively), for performing integration over radii in the application of the Mie theory to polydisperse aerosols.

These integrals give the scattering properties for a polydisperse collection of particles of identical optical constants, starting from the corresponding quantity for a single particle. They have the general form of an integral over the radius, from 0 to $\infty$, of the size distribution multiplied by the geometric cross section $\pi r^2$ of the particle and by an efficiency factor that is a limited function of $r$.

Nevertheless, any quadrature (i.e., numerical integration) method requires two finite integration limits, $r_{min}$ and $r_{max}$. These limits have to be selected to minimize the integration interval without loss in accuracy: This is, in principle, possible because the size distribution vanishes at $r = 0, \infty$.

The principle underlying the choice of $r_{min}$ and $r_{max}$ is to stop the integration or, in the discretized form, the sum, when the addition of new terms does not significantly vary the integral function. This selection is realized by means of the following criterion:

$$[dN(r)/dr]r^2 < \text{cutoff value}$$

$$\forall\, r > r_{max}, \forall\, r < r_{min}, \quad (5)$$

in which only the part of the integrand function that leads the trend to zero in both $r = 0$ and $r = \infty$ is tested.

The code was modified to find the interval of integration automatically, as shown.

As well as automatically selecting the extremes of the size range, users can choose to input different $r_{min}$

Table 3. Comparisons with Other Databases[a]

| Compared Databases | Test Case Description | | | | Results | |
|---|---|---|---|---|---|---|
| | Number of Parameters | Number of Wavelengths | Number of RH Levels | Number of Classes | Relative Difference <0.1% | Maximum Relative Difference (%) |
| SF | 3 | 4 | 3 | 2 | 70/72 | 0.11 |
| WCP-112 | 3 | 4 | 1 | 4 | 26/48 | 1.21 |
| DALME | 3 | 4 | 1 | 2 | 19/24 | 0.17 |

[a]The total number of tested cases is the product of the number of computed aerosol optical parameters times the number of tested wavelengths, RH levels, and aerosol classes.

and $r_{max}$ values if they are aware that particles outside a certain size range do not exist under particular conditions.

## 3. Database Validation

### A. Numerical Comparisons with Other Databases

The Database has been designed to provide the optical parameters of all the components and classes listed in Tables 1 and 2, respectively, which are called default or basic. The input data needed for the computations have been digitized and are contained in the input data set. The components and classes are taken from the most well-known and frequently used aerosol models, namely those proposed by (1) Shettle and Fenn,[2] (2) the World Climate Research Program in 1983,[6] (3) the same organization in 1986[7] (referred to as WCP-112), and (4) d'Almeida *et al.*[3] in 1991 (referred to as DALME).

To validate the output of the Database, tests have been carried out to compare the optical properties (extinction coefficient, single-scattering albedo, and asymmetry parameter) computed by the Database with corresponding results found in the literature, after a careful check on the equivalence of input parameters. Calculations have been performed across the UV–visible range at the following wavelengths: 0.300, 0.337, 0.500, and 0.694 μm.

The results of such comparisons are presented in Table 3. For each literature source, the number of selected cases (i.e., the product of the number of tested classes times the number of wavelengths times the number of humidity levels times the number of compared parameters) and the number of comparisons leading to a percentage error of less than 0.1% are presented along with the maximum difference found, regardless of the parameter, wavelength or RH at which the maximum occurred.

For the comparison with SF, the rural and the tropospheric classes have been reproduced for three humidity levels: 0%, 70%, and 99%. Almost all the compared values show a relative difference smaller than 0.1%; the largest relative difference found is 0.11%.

The accuracy in reproducing WCP-112 results has been tested considering the maritime, urban or industrial, volcanic 2, and background stratospheric 2 classes. The comparison is limited to dry (RH = 0%) conditions because no results are available from Ref. 7 for humid conditions.

Finally, clean continental and urban classes have been considered for the comparison with DALME results. In Table 3 only results obtained at the 0% RH level are presented. Comparisons at RH = 70% and 99% have been omitted because their discouraging results could be ascribed to "some errors in the tabulated Mie scattering calculations"[16] found in Ref. 3.

The validation of the phase function is treated separately. Because none of the above-mentioned sources present a phase-function tabulation to compare with the Database results, some phase functions published in Ref. 17 have been reproduced. More precisely, silicate haze M (at $\lambda$ = 0.589 μm for both refractive indices 1.55–$i$0.0155 and 1.55–$i$0.155, with a modified gamma distribution) phase functions have been tabulated for 30 angles in the 0°–180° range. The largest relative difference encountered in this comparison is 0.23%.

Overall the results of these comparisons are quite satisfactory, considering that small systematic differences in the extinction coefficients were expected because of the new automatic selection of the integration limits adopted [see inequality (5)], which leads, in general, to size ranges larger (i.e., smaller $r_{min}$ and greater $r_{max}$ values) than those reported in the literature and thus to greater values of $K^{ext}$. Percentage differences of less than 0.1% are considered negligible because they can be ascribed to different computation procedures and to different machine performances.

### B. Contrasts with Other Databases

Now that the Database has been validated by a comparison of numerical results, it is useful to show how the Database constitutes an attempt to overcome the practical difficulties with existing aerosol databases and to highlight which characteristics may be inadequate from the other cited databases.

First the Database contains all the components and classes available from the cited literature for which a complete set of information is available. The analytical forms of the size distributions are unified, and the meaning and the units of input parameters are unambiguous.

Mixtures made by chemically different or hygroscopic components can be built up as internal or ex-

ternal mixtures: None of the cited databases explicitly allow internal mixtures, with the exception of SF, in which components are made of internally mixed substances (see Subsection 2.B for details) but whose classes are obtained by means of external mixtures.

All the analyzed databases present aerosol-class optical characteristics for fixed component mixing ratios; only WCP-112 allows the weighting of component optical properties to compute those for externally mixed classes by varying mixing ratios. Our Database enlarges this to all the collected components, irrespective of mixing type. This is undoubtedly a gain in flexibility: Even a powerful database such as SF does not allow one to derive aerosol optical properties from models other than the predefined ones.

Each Mie computation leads to a result for the scattering phase function. WCP-112 and DALME do not provide this output.

The effect of humidity has been accounted for as described in Subsection 2.C. In this way it was possible to reproduce SF results and to investigate differences with those results contained in DALME. The use of this approach for humidity effects allows one to overcome the limitation of the WCP-112 scheme, which dealt with only dry aerosols.

### C. Applicability Limits

Tests showed that the code cannot deal with pure real refractive indices (no aerosol absorption). This has been compensated for by use of very low refractive-index imaginary parts ($\sim 10^{-9}$) (as seen below).

Finally, little effort is required for altering the current maximum limit (for internal mixing only) of a three-modal log-normal size distribution to achieve an arbitrary modality number.

### D. Test with Real Data

A further demonstration of the Database capability is the reproduction of measured aerosol optical depths. Villevalde *et al.*[18] presented results of a series of aerosol optical depth measurements made in the North Atlantic within a wide spectral range. They tested different aerosol models to fit the measured mean spectra. As a fitting criterion, they assumed that the measured and the calculated spectra should not differ by more than ±0.01 (measurement error) at each wavelength. They obtained calculated spectra by employing some bimodal size distributions with fixed log-normal distribution parameters and refractive-index values and by varying the component concentration and number-density mixing ratio. We assumed that the same input values found by Villevalde *et al.*[18] were successful in fitting measured data, and then we computed the same spectra by using our Database. The results are shown in Fig. 3.

Villevalde *et al.* did not use any of the Database default classes because they assumed that the particles were nonabsorbing spheres with a wavelength-independent real refractive index of 1.5. Thus, with the aim of reproducing their results, we used the selection of user-defined classes. Three classes were tested, which are labeled WCP-112, SF, and VILL (that of Villevalde *et al.*[18]). The former two presented the same size-distribution parameters that can be found in Refs. 7 and 2, respectively, whereas the latter has been entirely defined by Villevalde *et al.* to obtain physically acceptable concentrations. The summary of input data in our computations is given in Table 4. The refractive index is fixed at $1.5–i5.0 \times 10^{-9}$ in all cases. The following relations were used in computations:

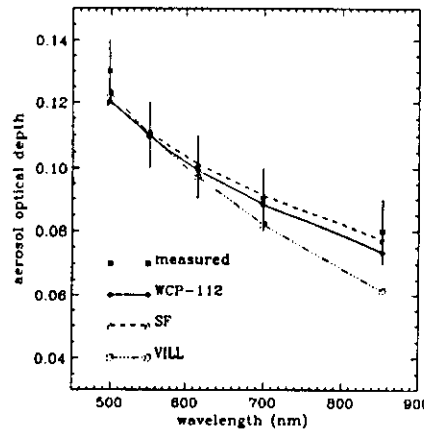


Fig. 3. Comparison of measured and calculated optical depth spectra. Vertical bars represent the fitting tolerance limits. VILL, input values of Villevalde *et al.*[18]

$$\tau_\lambda(\lambda) = K^{\mathrm{ext}}(\lambda)\ (\mathrm{km}^{-1}\ \mathrm{cm}^3) A\ (\mu\mathrm{m}^{-2}) \times 10^3, \qquad (6)$$

$$A = A_f + A_c, \qquad n_f = A_f/A, \qquad n_c = A_c/A, \qquad (7)$$

where $A$ is the aerosol columnar abundance and $n_f$ and $n_c$ are the fine and the coarse mode number-density mixing ratios, respectively.

The exercise can be considered successful even if the VILL class did not satisfy the fitting criterion at 853 nm.

## 4. Application

Several authors[6,11] have highlighted the sensitivity of aerosol radiative response to assumptions about mixing type. This sensitivity is important because the response is related to aerosol-climate problems as well as to aerosol-detection tasks. We decided to perform a Database exercise to investigate the quantitative differences in aerosol-class optical properties.

Table 4. Parameters of Size Distributions and Aerosol Abundances Employed in Fitting Measurements by Villevalde *et al.*[18]

| Mode | Parameter | WCP-112 | SF | VILL |
|---|---|---|---|---|
| Fine | $r_m$ (μm) | 0.005 | 0.03 | 0.08 |
| | σ | 0.476 | 0.350 | 0.2304 |
| | $A_f$ ($\mu\mathrm{m}^{-2}$) | 161.2 | 6.48 | 1.69 |
| Coarse | $r_m$ (μm) | 0.3 | 0.3 | 1.0 |
| | σ | 0.400 | 0.400 | 0.0792 |
| | $A_c$ ($\mu\mathrm{m}^{-2}$) | 0.007 | 0.010 | 0.003 |

Table 5. Spectral Refractive Indices of the Examined Aerosol Components[a]

| Wl (nm) | Water Soluble 1 Real | Water Soluble 1 Imaginary ($\times 10^{-3}$) | Dustlike 1 Real | Dustlike 1 Imaginary ($\times 10^{-3}$) | Soot Real | Soot Imaginary ($\times 10^{-1}$) | Oceanic Real | Oceanic Imaginary |
|---|---|---|---|---|---|---|---|---|
| 300.0 | 1.530 | −8.00 | 1.530 | −8.00 | 1.740 | −4.70 | 1.395 | $-5.83 \times 10^{-7}$ |
| 400.0 | 1.530 | −5.00 | 1.530 | −8.00 | 1.750 | −4.60 | 1.385 | $-9.90 \times 10^{-9}$ |
| 550.0 | 1.530 | −6.00 | 1.530 | −8.00 | 1.750 | −4.40 | 1.381 | $-4.26 \times 10^{-9}$ |
| 694.0 | 1.530 | −7.00 | 1.530 | −8.00 | 1.750 | −4.30 | 1.376 | $-5.04 \times 10^{-8}$ |

[a]Water soluble 2 and water soluble 1 do not differ in spectral refractive indices.

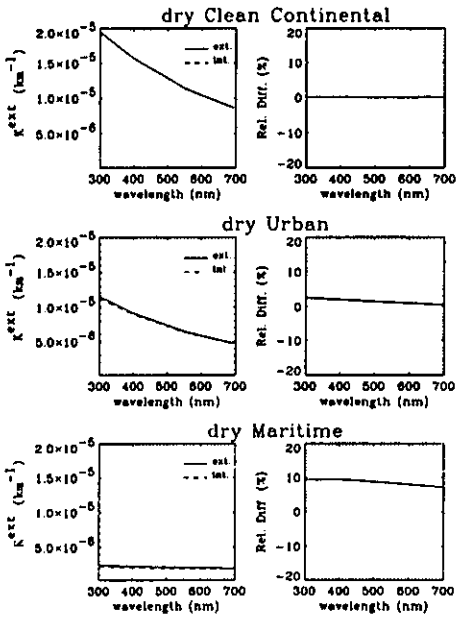


Fig. 4. Left: spectral extinction coefficients (at 1 particle/cm$^3$) of externally and internally mixed aerosol classes. Right: spectral percentage differences between the two quantities.

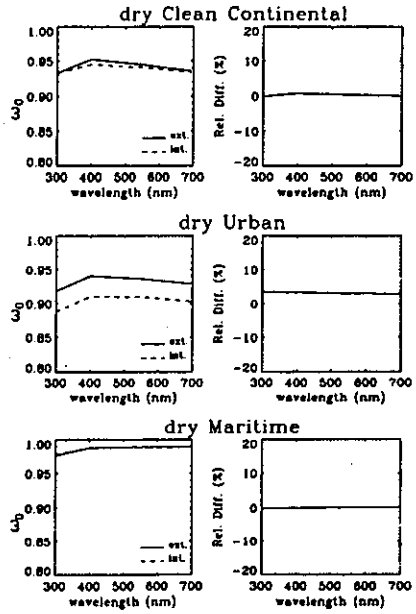


Fig. 5. Left: spectral single-scattering albedo values of externally and internally mixed aerosol classes. Right: spectral percentage differences between the two quantities.

We computed the spectral specific extinction coefficient (1 particle/cm$^3$) and single-scattering albedo for three internal and external mixtures: clean continental, maritime, and urban. Data input were selected at a RH of 0% with a wavelength extending across the UV–visible range (four values; see Table 5).

Results of the computations are presented for each optical variable (Figs. 4 and 5) as functions of wavelength; both absolute values and relative differences between the optical properties of external and internal mixture are shown. The behavior of relative differences for each aerosol class is assessed separately.

Nevertheless, some aspects of internal and external mixed optical properties must be kept in mind: The extinction coefficient and the single-scattering albedo of an externally mixed aerosol class were obtained as weighted averages of the same optical properties (as described in Appendix A) and were computed separately for each aerosol component (Fig. 6). Optical properties of internally mixed classes depend on the unique refractive index computed as a volume-weighted average (Table 6). Note that differences in differently mixed aerosol optical properties do not present any significant spectral dependence on the selected wavelength range for all the classes tested.

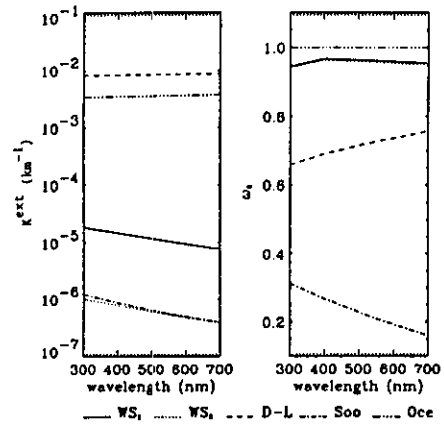


Fig. 6. Examined aerosol dry components. Left: spectral extinction coefficients (at 1 particle/cm$^3$). Right: spectral single-scattering albedo values. $WS_1$, water soluble 1; $WS_2$, water soluble 2; D–L, dustlike; Soo, soot; Oce, oceanic.

Table 6. Spectral Refractive Indices for Examined Internally Mixed Aerosol Classes

| | Clean Continental | | Urban | | Maritime | |
|---|---|---|---|---|---|---|
| Wl (nm) | Real | Imaginary ($\times 10^{-3}$) | Real | Imaginary ($\times 10^{-2}$) | Real | Imaginary ($\times 10^{-4}$) |
| 300.0 | 1.530 | −8.00 | 1.535 | −1.82 | 1.402 | −4.01 |
| 400.0 | 1.530 | −6.56 | 1.535 | −1.50 | 1.392 | −2.50 |
| 550.0 | 1.530 | −7.04 | 1.535 | −1.56 | 1.388 | −3.00 |
| 694.0 | 1.530 | −7.52 | 1.535 | −1.63 | 1.384 | −3.50 |

### A. Clean Continental

As is clearly shown in Figs. 4 and 5, the effect of selecting a different mixing type is almost negligible as far as the present investigation of the clean continental aerosol optical properties is concerned. The result is due to the fact that the water-soluble component is dominant in particle number density in both external and internal mixing. Moreover, spectral refractive indices are identical for the two components involved.

### B. Urban

The single-scattering albedo is the fraction of energy removed from the incident radiation, which reappears as scattered radiation. It is evident (Fig. 5) that this parameter is higher for the external mixture than for the internal one.

This can be explained by considering that the single-scattering albedo for an external mixture is the result of the weighted average of the component single-scattering albedo values [see Eq. (A2)]. The weightings are the mixing ratios by particle number density and the extinction coefficients. Even though soot and dustlike components show the strongest absorbing potential (Fig. 6, right-hand side), the influence of both is weakened by very small weights (from 1 to 3 orders of magnitude less than the weight of the water soluble 1 component) resulting from the number-density mixing ratio for the dustlike components (6 orders of magnitude lower than those of the other two components; see Table 7), and the specific extinction coefficient for soot (Fig. 6, left-hand side).

As far as internal mixture is concerned, it is no longer possible to evaluate explicitly each component weight when determining the single-scattering albedo values, because the mixture has to be considered in this case as composed of nondistinguishable particles with a unique refractive index and a three-modal size distribution. Nevertheless, it can be stated that soot plays a relevant role in causing the internal mixture to absorb more than the external one. In fact, soot determines the relatively high values of the imaginary part of the refractive index of the urban mixture (Table 6) if they are compared with those of the other two classes tested. Such values resulted from the weighted average of the imaginary parts of the component refractive index, following Eq. (A4), by use of data from Tables 7 (column 3) and 5 as input.

As opposed to the case of external mixing, in which soot had a low probability of acting as an absorber because of its low specific extinction coefficient, here soot gives major evidence of its absorbing potential by means of the imaginary part of the refractive index of the mixture.

### C. Maritime

In contrast to the urban case, the maritime aerosol is composed of quasi-nonabsorbing components (note that the water-soluble component differs in size distribution with respect to that considered above). The fact that the single-scattering albedo values are almost equal is not surprising. Even though the different mixing type does affect the extinction coefficient values, the differences are small.

## 5. Summary and Concluding Remarks

A database of aerosol optical properties (extinction, scattering, and absorption coefficients, phase function, asymmetry factor, and single-scattering albedo) has been presented. The input data set of physical properties of default components is based on widely recognized and frequently used aerosol models. Optical properties of default classes as well as user-defined classes can be obtained from the Database. RH effects are accounted for, allowing computations from dry (RH = 0%) to very wet (RH = 99%) conditions. Both of these possible mechanisms for mixing components, internal or external mixing, are available.

Aerosol optical properties computed by means of

Table 7. Examined Aerosol-Class Input Data

| Class | Component | Mixing Ratio by Volume | Mixing Ratio by Number | Size-Distribution Parameters | |
|---|---|---|---|---|---|
| | | | | $r_m$ (μm) | $\sigma$ |
| Clean continental | Water soluble 1 | 0.48 | 0.9999 | 0.0285 | 0.350 |
| | Dustlike 1 | 0.52 | $1.0 \times 10^{-4}$ | 0.471 | 0.400 |
| Urban | Water soluble 1 | 0.975 | 0.5945 | 0.0285 | 0.350 |
| | Dustlike 1 | 0.003 | $1.67 \times 10^{-7}$ | 0.471 | 0.400 |
| | Soot | 0.022 | 0.4055 | 0.0118 | 0.301 |
| Maritime | Water soluble 2 | 0.05 | 0.99958 | 0.005 | 0.476 |
| | Oceanic | 0.95 | 0.00042 | 0.3 | 0.400 |

the Database allow simulation of spectral solar radiance diffusion by the atmosphere. By comparing computed radiance with radiance measured by remote sensing, it is possible to select the aerosol model that best reproduces the spectral variations and the angular distribution of those measurements. Such a method is often called a pseudoinversion method, as it allows one to determine the aerosol characteristics without a mathematical inversion of the radiative transfer equation. Algorithms have to satisfy different requirements related to different types of measurement (instrument type and location, spatial and spectral resolution, etc.). It is beyond the scope of this paper to discuss details of such algorithms, which primarily depend on which main physical phenomena (other than aerosol radiative effects) influence the measured radiance: Note, for example, that the presence of highly reflecting Earth surfaces (nadir-viewing instruments) as well as clouds will prevent retrieval of aerosol information when passive-remote-sensing measurements are used.

It is intended to use the Database to develop the retrieval of aerosol optical thicknesses for the Global Ozone Monitoring Experiment, a spectrometer that measures radiance reflected from the Earth's atmosphere in the UV–visible spectral range, which is currently flying on the ERS2 satellite.

The Database should prove to be a powerful tool in those studies whose aim is to measure the aerosol optical properties (e.g., optical thickness and columnar size distribution).

## Appendix A

*External mixing:* The optical properties of an aerosol class, as a weighted average of the components optical properties, are given by

$$K^{\text{ext,sca,abs}} = \frac{\sum_j n_j K_j^{\text{ext,sca,abs}}}{\sum_j n_j} \tag{A1}$$

$$\omega_0 = \frac{\sum_j n_j K_j^{\text{ext}} \omega_{0_j}}{\sum_j n_j K_j^{\text{ext}}} \tag{A2}$$

$$P(\gamma) = \frac{\sum_j n_j K_j^{\text{sca}} P_j(\gamma)}{\sum_j n_j K_j^{\text{sca}}}, \tag{A3}$$

where $j$ refers to each component, $n_j$ is the particle number-density mixing ratio, $K^{\text{ext,sca,abs}}$ is the specific extinction (scattering, absorption) coefficient, $\omega_0$ is the single-scattering albedo, and $P(\gamma)$ is the phase function; the asymmetry factor is weighted analogously.

*Internal mixing:* The refractive index of an aerosol class as a volume-weighted average of components refractive indices is given by

$$m = \frac{\sum_j v_j m_j}{\sum_j v_j}, \tag{A4}$$

where $m$ is the complex refractive index of the class, $m_j$ is the complex refractive index of the $j$th component, and $v_j$ is the volume mixing ratio, which is derived as

$$v_j = 4/3\pi n_j \int_0^\infty r^3 (dN/dr) dr$$

$$= 4/3\pi n_j r_{m_j}^3 \times \exp\left[\frac{9}{2}\left(\frac{\sigma_j}{\log(e)}\right)^2\right]. \tag{A5}$$

The database, along with all relevant input files and software tools, is available on request from R. Guzzi (e-mail address: guzzi@imga.bo.cnr.it). The authors are grateful to Eric P. Shettle for helpful suggestions regarding internal and external mixing and on the use of the MIE2 code. C. Levoni and F. Torricella are supported by European Space Agency contract 11572/95/NL/CN.

## References

1. S. Twomey, "The influence of pollution on the shortwave albedo of clouds," J. Atmos. Sci. **34**, 1149–1152 (1977).
2. E. P. Shettle and R. W. Fenn, "Models for the aerosol lower atmosphere and the effects of humidity variations on their optical properties," Rep. Tr-79-0214 (U.S. Air Force Geophysics Laboratory, Hanscom Air Force Base, Mass., 1979).
3. G. A. d'Almeida, P. Koepke, and E. P. Shettle, *Atmospheric Aerosols. Global Climatology and Radiative Characteristics* (Deepak, Hampton, Va., 1991).
4. O. B. Toon and J. B. Pollack, "A global average model of atmospheric aerosol for radiative transfer calculations," J. Appl. Meteorol. **15**, 225–246 (1976).
5. R. W. Fenn, "Aerosol-Verteilungen und atmospharisches Streulicht," Beitr. Phys. Atmos. **37**, 69–104 (1964).
6. A. Deepak and H. E. Gerbers, eds., "Report of the experts' meeting on aerosols and their climatic effects," WCP-55 (World Climate Research Program, Geneva, 1983).
7. World Meteorological Organization, "A preliminary cloudless standard atmosphere for radiation computation," WCP-112 (World Climate Research Program, CAS, Radiation Commission of IAMAP, Boulder, Colo., 1986).
8. M. Wang and H. R. Gordon, "Radiance reflected from the ocean-atmosphere system: synthesis from individual components of the aerosol size distribution," Appl. Opt. **33**, 7088–7095 (1994).
9. A. M. Ignatov, L. L. Stowe, S. M. Sakerin, and G. K. Korotaev, "Validation of the NOAA/NESDIS satellite aerosol product over the North Atlantic in 1989," J. Geophys. Res. **100**, 5123–5132 (1995).
10. F. Dulac, D. Tanré, G. Bergametti, P. Buat-Ménard, M. Desbois, and D. Sutton, "Assessment of the African airborne dust mass over the western Mediterranean Sea using Meteosat data," J. Geophys. Res. **97**, 2489–2506 (1992).
11. J. M. Haywood and K. P. Shine, "The effect of anthropogenic sulfate and soot aerosol on the clear sky planetary radiation budget," Geophys. Res. Lett. **22**, 603–606 (1995).

12. M. I. Mishchenko, A. A. Lacis, B. E. Carlson, and L. D. Travis, "Nonsphericity of dustlike tropospheric aerosol: implication for aerosol remote sensing and climate modeling," Geophys. Res. Lett. **22**, 1077–1080 (1995).
13. F. X. Kneizys, E. P. Shettle, W. O. Gallery, J. H. Chetwind, L. W. Abreu, J. E. A. Selby, S. A. Clough, and R. W. Fenn, "Atmospheric transmittance/radiance: the LOWTRAN 6 model," Rep. AFGL-83-0187, NTIS AD A137796 (U.S. Air Force Geophysics Laboratory, Hanscom Air Force Base, Mass., 1983).
14. G. Hanel, "The properties of atmospheric aerosol particles as functions of the relative humidity at thermodynamic equilibrium with the surrounding moist air," Adv. Geophys. **19**, 73–188 (1976).
15. G. Hänel, "The physical chemistry of atmospheric particles," in *Hygroscopic Aerosol*, L. H. Ruhnke and A. Deepak, eds. (Deepak, Hampton, Va., 1984), pp. 1–20.
16. E. P. Shettle, Remote Sensing Division, U.S. Naval Research Laboratory, Washington, D.C. 20375 (personal communication, 1996).
17. D. Deirmendjian, *Electromagnetic Scattering on Spherical Polydispersions* (Elsevier, New York, 1969), pp. 151–285.
18. Yu. V. Villevalde, A. V. Smirnov, N. T. O'Neill, S. P. Smyshlyaev, and V. V. Yakovlev, "Measurement of aerosol optical depth in the Pacific Ocean and the North Atlantic," J. Geophys. Res. **99**, 20983–20988 (1994).

Reprinted from Applied Optics, Vol. 21, page 1578, May 1, 1982
Copyright © 1982 by the Optical Society of America and reprinted by permission of the copyright owner.

# Aerosol size spectra from spectral extinction data: the use of a linear inversion method

R. Rizzi, R. Guzzi, and R. Legnani

A modification of the Twomey-Phillips linear constrained inversion method is used to retrieve aerosol size spectra from simulated spectral optical depths in the wavelength range from 0.37 to 2.2 $\mu$m. It is found that the transition between nonphysical solutions to well-behaved ones, which is driven by the smoothing parameter $\gamma$, is gradual and that negative components, when present in the solution, always belong to the smallest particle range. When values of $\gamma$ greater than 0.05 are required to obtain well-behaved solutions, a strong bias on the retrieved solution is posed by the form of the first-guess solution. Moreover, even if the retrieved size distribution computed for low values of $\gamma$ is not well-behaved, much information on the shape of the true solution in the medium and large particle range is contained in the retrieved solution. The effect of realistic random errors added to the simulated optical depths is also discussed.

## I. Introduction

Aerosols affect the atmospheric and terrestrial heat budget by absorbing and scattering shortwave radiation and by emitting and scattering longwave infrared radiation. Their influence on radiation depends primarily on the physical characteristics: refractive index, size, and geometrical shape. Were these parameters known with some accuracy, the exact mathematical solutions of the transfer equation for a turbid atmosphere could be computed.

Much information regarding the aerosol microstructure and the density variation with height has been assembled: the work by Shettle and Fenn,[1] Blifford and Ringer,[2] Hofmann *et al.*,[3] Rosen *et al.*,[4] and Cress[5] in this respect represents extremely important steps. However there is still a great need to improve methods which permit the determination of some properties of particulate matter and to standardize those that appear most reliable. The temporal and spatial resolution of the set of data necessary to describe all the features of aerosol relevant to atmospheric optics must be improved to cope with the standards achieved in dealing with other phenomena which are incorporated in dynamic models.

Our attention is focused on the determination of aerosol size distributions by indirect methods using spectral extinction measurements. The problem has been examined by several authors. A list of references together with a description of the methods and results can be found in King *et al.*[6] Their paper deserves attention since it represents an attempt to tackle several problems that are encountered when linear constrained methods are used to retrieve optical depths, that is, (1) the introduction of information on the experimental error inside the algorithm; (2) the dependence of the retrieval solution on the first-guess solution; (3) the choice of the radius range to be used in the inversion; (4) the choice of the best values of the smoothing parameter; and (5) the influence of the generally poor knowledge of the aerosol refractive index on the retrieval solution.

These problems are, to some extent, still research subjects, as the objective of defining a set of data handling procedures to compute aerosol size spectra is not yet fulfilled. Our paper is structured in such a way to use figures as the most relevant vehicle of information leaving the printed matter to connect the shown results.

## II. General Definition of the Problem

Direct solar monochromatic irradiance $I(\lambda)$ is computed using the relation

$$I(\lambda) = I_0(\lambda) \exp[-\tau(\lambda) \cdot m],$$

where $I_0(\lambda)$ is the extra-atmospheric irradiance at wavelength $\lambda$, $\tau(\lambda)$ is the optical depth, and $m$ is the air mass.

R. Guzzi is with FISBAT-CNR, Bologna, Italy; the other authors are with Istituto di Geofisica dell'Universita degli Studi, 40125 Bologna, Italy.

Received 26 June 1981.
0003-6935/82/091578-10$01.00/0.
© 1982 Optical Society of America.

The optical depth $\tau(\lambda)$ describes the modes of interaction between radiation and atmospheric matter and can be expressed as the sum of optical depth $\tau_a(\lambda)$ due to the presence of particulate matter, Rayleigh scattering $\tau_R(\lambda)$, and absorption by water vapor $\tau_{wv}(\lambda)$ and by other gases (such as $O_3$,$O_2$) contained in the atmosphere $\tau_g(\lambda)$.

If measurements of precipitable water are available (see, for example, Tomasi and Guzzi[7]), it is possible to derive $\tau_a(\lambda)$ as

$$\tau_a(\lambda) = \frac{1}{m} \ln \frac{I_0(\lambda)}{I(\lambda)} - \tau_R(\lambda) - \tau_g(\lambda) - \tau_{wv}(\lambda), \quad (1)$$

since the terms on the right-hand side of Eq. (1) can be either measured or computed from data taken from the literature.

The particulate matter optical depth is usually computed by

$$\tau_a(\lambda) = \int_0^\infty \int_0^\infty \pi r^2 Q_E(r,\lambda,m) n(r,h) dr dh, \quad (2)$$

where $n(r,h)$ is the aerosol differential size distribution at height $h$, $Q_E(r,\lambda,m)$ is the Mie extinction coefficient[8] of a spherically homogeneous particle of radius $r$ and complex refractive index $m$. Measurements of aerosol concentration show that the vertical variation can be described by a piecewise linear curve in semilogarithmic scale.[9] Moreover if the aerosol size distribution is assumed independent of height but for a multiplicative factor, the integral in Eq. (2) is separable and can be written as

$$\tau_a(\lambda) = \pi H_D \int_0^\infty r^2 Q_E(r,\lambda,m) n(r) dr, \quad (3)$$

where $H_D$ is the aerosol scale height whose value is assumed equal to $10^5$ cm. The implications of the last simplifying assumption will be discussed in Sec. V. For convenience Eq. (3) can be written in terms of $x = \log r$, following the procedure adopted by King *et al.*[6] Then the optical depth is expressed as

$$\tau_a(\lambda) = \pi H_D \int_{x_I}^{x_F} 10^{2x} Q_E(10^x,\lambda,m) \frac{dN(x)}{dx} dx,$$

where the integration limits $(-\infty,+\infty)$ are replaced by $(x_I,x_F)$.

The size distribution function can be expressed, following King *et al.*[6] as

$$n(x) \equiv \frac{dN(x)}{dx} = t(x) \cdot f(x) \quad (\mathrm{cm}^{-4}),$$

where $f(x)$ is a smoothly varying function of $x$. Then Eq. (3) becomes

$$\tau_a(x) = \int_{x_I}^{x_F} K(\lambda,x) f(x) dx, \quad (4)$$

$$K(\lambda,x) = \pi H_D Q_E(10^x,\lambda,m) \cdot t(x) \cdot 10^{2x}. \quad (5)$$

The wavelength range of interest for the computations in this paper is from 0.37 to 2.2 $\mu$m. Twelve wavelengths (0.37, 0.44, 0.5, 0.52, 0.55, 0.68, 0.74, 0.93, 1.03, 1.25, 1.6, and 2.2) are selected which lie in regions of weak $H_2O$ absorption. The choice of the twelve wavelengths is made to simulate the behavior of a relatively simple filter radiometer devoted to aerosol and solar energy monitoring.

For a definition of the numerical values of the refractive index $m$ we refer to the rural aerosol model[1] composed of 70% soluble salts and 30% dust. It has been shown[10] that the extinction of shortwave and near-infrared radiation computed using a mean refractive index has a small deviation from that computed using the superposition of two aerosols with different refractive indices. Moreover, since the effect of the real and imaginary parts becoming smaller compensate each other in the computation of the extinction coefficient in the wavelength range of interest, a value of $m = (1.5,0)$ is chosen in the whole spectral range.

The system of twelve integral equations, each one like Eq. (4) for each value of $\lambda$, can be reduced to a system of linear independent equations by choosing $M$ quadrature points

$$x_i \in (x_I,x_F) \quad i = 1,M,$$
$$x_1 = x_I, \quad x_M = x_F.$$

Assuming that the function $f(x)$ is a piecewise linear function

$$f(x) = C_i + d_i x, \quad x \in (x_i,x_{i+1}), \quad i = 1,M-1,$$

it is possible to write

$$\int_{x_I}^{x_F} K(\lambda,x) f(x) dx \simeq \sum_1^M a_{ji} f_i, \quad (6)$$

where $f_i \equiv f(x_i)$ and the $a_{ji}$ are given in explicit form in Twomey.[11]

The final form of Eq. (4) is

$$\tau = \mathrm{A} \cdot \mathrm{f}, \quad (7)$$

where

$$\tau \equiv [\tau_a(\lambda_1), \ldots, \tau_a(\lambda_N)],$$
$$\mathrm{f} \equiv [f(x_1), \ldots, f(x_M)],$$
$$(\mathrm{A})_{ji} = a_{ji}.$$

In the following the vector $\tau$ will denote the simulated true measurements and the vector $\tau'$ the retrieved optical depths. Moreover the same letter is used to define a given function and the associated vector:

$$\mathrm{t} \equiv (t_1, \ldots, t_M) = [t(x_1), \ldots, t(x_M)],$$
$$\mathrm{f}' \equiv (f'_1, \ldots, f'_M),$$
$$\mathrm{n}' \equiv (n'_1, \ldots, n'_M) = (t_1 f'_1, \ldots, t_M f'_M),$$

where the vectors t, f', and n' denote, respectively, the first-guess solution, the retrieved solution, and the retrieved differential size distribution.

## III. Independence of a Set of Measurements

To determine the independence of the set of optical depths for the twelve wavelengths already defined, it is necessary to analyze (a) the shape of the kernel functions defined by Eqs. (5)and (6), and (b) the types of error involved in actual measurements. First it has to be noted that the choice of the integration interval

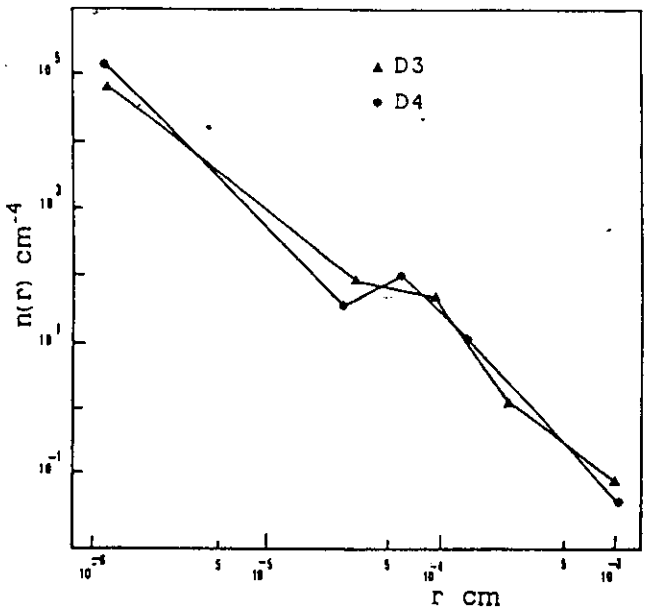


Fig. 1. Differential size distribution $n(x) = dN/d\log r$ plotted vs radius expressed in centimeters.

$(x_I, x_F)$ depends on the actual aerosol size distribution and therefore an *a priori* choice is not possible.

To choose a first-guess interval to be used in the computations and to be modified according to their results, the kernels $K(\lambda,x)$ were computed for various size distributions. Some of them (Junge *et al.*[12] and Deirmendjian[13] denoted as haze $M$, haze $L$, and haze $H$) are standard distributions and their definitions can be found in all textbooks dealing with atmospheric optics. Other distributions, called $D3$ and $D4$ and shown in Fig. 1, were used to apply the inversion technique to spectra of a size likely to be found in actual measurements. A qualitative analysis of the curves shows that a safe interval is for a radii ranging from 0.1 to 5.0 $\mu$m. For most distributions the interval can be shifted safely to 10 $\mu$m, while in some cases it can be extended to include smaller particles.

A similar problem is noted in the paper by King *et al.*[6] in which the possibility of extending the radius range is examined qualitatively in terms of the shape of the kernels. Certainly a significantly nonzero kernel at some wavelength is a necessary condition to ensure the possibility of a retrieval of a given size distribution. However there are cases in which the shape of a significant kernel changes only slightly with wavelength; in other words, the set of $\tau$ has a low degree of independence and it is extremely difficult to obtain good retrieval.

If $\varepsilon'$ is the error vector of actual measurements we may write $\tau = \mathrm{A}f' + \varepsilon'$. This relation can also be written as $1 = \mathrm{C}^{-1/2}\mathrm{A}f' + \varepsilon$, where $1 = (1,1,\ldots,1)$,

$$\mathrm{C} = \begin{vmatrix} \tau_1^2 & 0 & & & \\ 0 & \tau_2^2 & & & \\ & & & 0 & \\ & & 0 & & \tau_N^2 \end{vmatrix},$$

and the components of $\varepsilon$ are the percentage errors of actual measurements. Since the estimated percentage errors in the computation of aerosol optical depths from actually measured data have about the same numerical value in the wavelength range of interest, we assume that the errors $\varepsilon$ are uncorrelated and that in each channel the distribution of errors is normal with zero mean and variance $\sigma$.

It has been shown that the number of independent measurements of the whole set of $\tau$ is equal to the number of eigenvalues for which $\mu \gg \sigma^2$, where $\mu$ denotes an eigenvalue of the real symmetric matrix $\mathrm{A}^T\mathrm{C}^{-1}\mathrm{A}$ (the superscript T denotes transposition). The eigenvalue analysis of the matrices $\mathrm{A}^T\mathrm{C}^{-1}\mathrm{A}$ computed using several size distributions is shown in Fig. 2. The number $N$ in the abscissa denotes the number of simulated measurements used, i.e., six means that kernels and optical depths were computed at 0.37, 0.44, 0.5, 0.52, 0.55 and 0.68-$\mu$m wavelengths. Hence as $N$ increases, the wavelength range is extended toward the near infrared. The value of the eigenvalue $\mu$ for a given size distribution and value of $N$ is on the ordinate scale. The segments connecting the eigenvalues are drawn only to allow a better comprehension of the plotted data.

The assumption on the magnitude of $\sigma$ is quite critical to decide on how many pieces of information are available. During the simulations a correspondence between the accuracy of the retrieved solution and the available information has been noted.

## IV. Method

### A. General Definition

The system of Eq. (7) is solved using the technique developed by Phillips[14] and Twomey[15,16] and used by Yamamoto and Tanaka.[17] It consists of solving a problem of constrained minimization, that is, to find a vector f′ which minimizes the quadratic form $q = f'^T H f'$ with the constraint: distance $(\tau, \mathrm{A}f') \leq \eta$.

The M × M real symmetric matrix H is constructed so that the quadratic form $q$ defines a measure of smoothing of f′ and that $\eta$ is a measure of the experimental error. The matrix H is defined as

$$\mathrm{H} = \begin{vmatrix} 1 & -2 & 1 & 0 & 0 & 0 \\ -2 & 5 & -4 & 1 & 0 & 0 \\ 1 & -4 & 6 & -4 & 1 & 0 \\ 0 & 1 & -4 & 6 & -4 & 1 \\ 0 & 0 & 1 & -4 & & \\ 0 & 0 & 0 & 1 & & \end{vmatrix}$$

Therefore $q$ is the sum of the second differences of f′. In the whole set of computations the distance between retrieved and actual optical depths is defined as

$$d_\tau^2 = \delta^2(\tau',\tau,N) \equiv \frac{1}{N}\sum_1^N j\left(\frac{\tau_j' - \tau_j}{\tau_j}\right)^2. \tag{8}$$

This choice allows an evaluation of $\eta$. Given two vectors $\tau$ and Af′ for which

$$\left|\frac{(Af')_j - \tau_j}{\tau_j}\right| \leq \sigma, \qquad J = 1,N,$$

we have that $\delta(Af',\tau,N) \leq \sigma$.

The solution to the problem formerly posed is obtained with the Lagrange multipliers method:

$$f' = (A^TC^{-1}A + \gamma H)^{-1}A^TC^{-1}\tau, \tag{9}$$

where $\gamma$ is an undetermined Lagrange multiplier. The symbol $^{-1}$ applied to a matrix means the evaluation of the inverse form of the matrix itself.

If $\gamma$ is chosen equal to zero, Eq. (9) is equivalent to a direct inversion of a quasi-singular matrix A with more than one eigenvalue near zero. The effect of these eigenvalues is to amplify small differences between the $\tau$ and to produce dramatically different solutions $f'$. As $\gamma$ increases the smallest eigenvalues of $A^TC^{-1}A$ are filtered out and some information is *de facto* inserted into the system, the effect of which is to remove the indetermination.[18]

## B. Initialization Procedure

A least squares fit of the synthetic optical depths $\tau$ is accomplished assuming that the first-guess solution $t(x)$ is a Junge, haze $M$, haze $L$, and haze $H$ size distribution. Then the distances [computed according to Eq. (8)] between the obtained optical depths $\tau'$ and the true depths $\tau$ are computed, and t is chosen which minimizes this distance. For the Junge-type size distributions both parameters are computed, taking into account the limited radius range in which $t(x)$ is defined, while only the normalization parameter is left free to vary for the Deirmendjian models. The least squares fit can be applied to a selected number of $\tau$ starting from the one computed at lowest wavelength or to the whole set of $\tau$. This is done to possibly extract from the $\tau$ information about the shape of $n(x)$ in the smallest radius range.

## C. Examples of Inversion with Error-Free Optical Depths

The linear method described in Sec. IV.A produces solutions (for values of $\gamma$ from $10^{-10}$ to 1) such that the distance $d_\tau$ between the measured and retrieved optical depths usually has a monotonic increasing behavior if plotted vs $\gamma$. Hence the distance $d_\tau$ is not by itself a sufficient condition on which to decide whether the solution is good. Another constraint which can be posed is that the solution vector $f'$ be positive definite because of its physical meaning.

When dealing with simulated data, as in our case, the distance between distributions can also be defined and used as a discriminating parameter. The choice of distance has no impact on the solution since it is not incorporated into the technique but may prove a nice tool to correctly interpret the results of the experiments if it is somehow linked to the definition of distance between optical depths.

Let us assume that the $N$ kernels $K(\lambda_j,x)$ [which incorporate the first-guess solution $t(x)$] follow a normal distribution whose variance is $v$:

$$K(\lambda_j,x) = \frac{1}{\sqrt{2\pi}} \exp\left[-\frac{1}{2}\left(\frac{x-\zeta_j}{v}\right)^2\right],$$

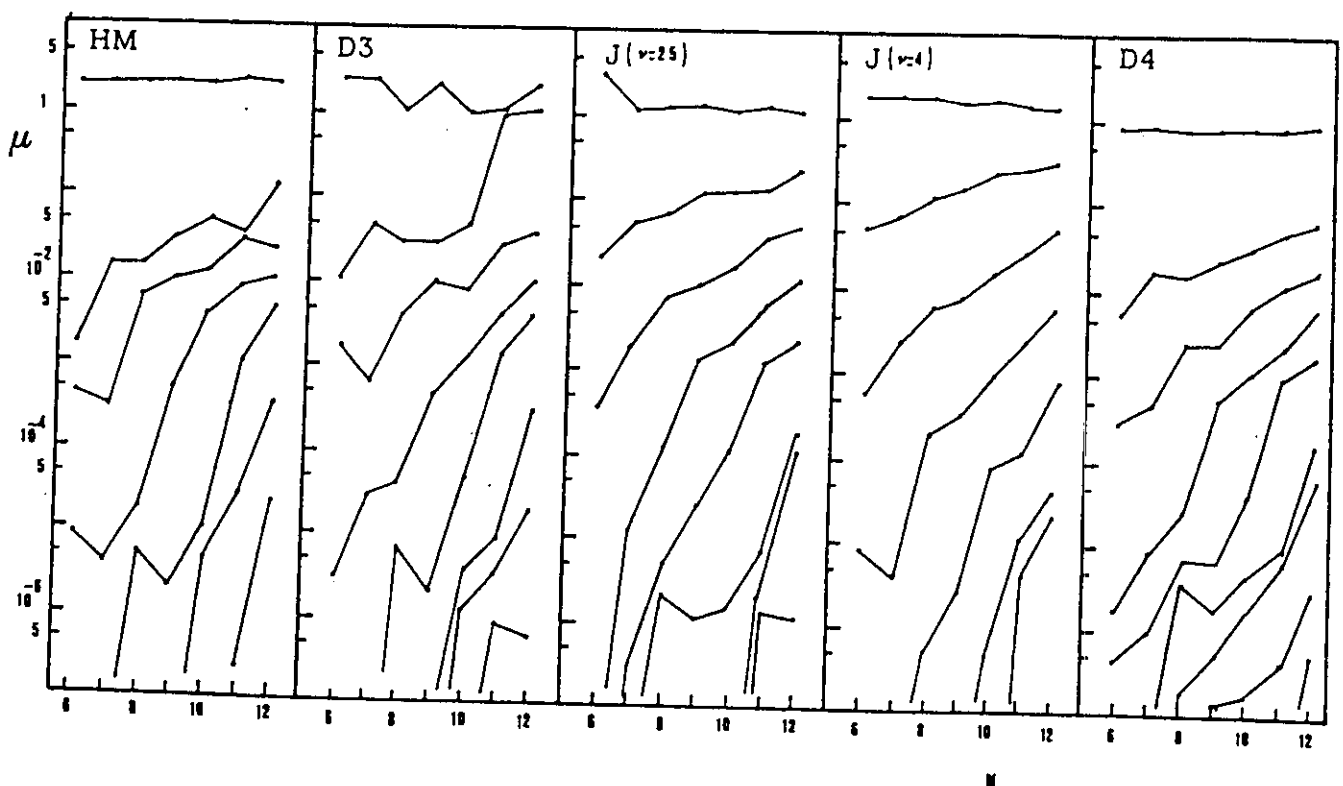


Fig. 2. Largest eigenvalues $\mu$ plotted vs number $N$ of measurements. Computations are done for the following size distributions: HM (Deirmendjian haze $M$); J (Junge, whose exponent $\nu$ is specified in the figure); $D3$ and $D4$ (shown in Fig. 1).

and that the function $f(x)$ is linear on a semilogarithmic scale $f(x) = a_0 + a_1 \cdot x$. The true size distribution is $n(x) = t(x) \cdot f(x)$.

Under these assumptions it can be proved that $\tau_j = \pi H_D \sqrt{v^2} f(\zeta_j)$. This relation allows one to compute the size distribution at $\zeta_j$ [the value of $x$ at which $K(\lambda_j,x)$ has the maximum] when the corresponding optical depth is known. Let us assume that the retrieved vector $\mathbf{f}'$ is linear with coefficients $a_0'$ and $a_1'$. The retrieved optical depths are $\tau_j' = \pi H_D \sqrt{v^2} f'(\zeta_j)$. Therefore the distance [Eq. (8)] can be expressed as

$$d_\tau^2 = \frac{1}{N} \sum_1^N {}_j \left[ \frac{f'(\zeta_j) - f(\zeta_j)}{f(\zeta_j)} \right]^2 .$$

It is therefore plausible to define a distance between the size distributions as

$$d_n^2 = \delta^2(\mathbf{n}',\mathbf{n},N) = \frac{1}{N} \sum_1^N {}_k \left[ \frac{n_k' - n(x_k)}{n(x_k)} \right]^2 . \tag{10}$$

The approximation of the shape of the kernel can be considered adequate for our purpose for many types of functions $t(x)$, Junge, Deirmendjian, and even $D3$ and $D4$. The assumption of the linearity of the $f(x)$ is by no means restrictive since in actual simulations $f(x) = 1$ ($x_I \le x \le x_F$). More restrictive is the assumption on the retrieved $\mathbf{f}'$ since it means that we are dealing with a good first-guess solution $\mathbf{t}$ or that the retrieval is made for a large value of $\gamma$. Moreover it is shown that, under the stated approximation, there is a relation between optical depths and solutions measured at the point $\zeta_j$ but not at any $x_j$ point.

The relation between $\tau_j'$ and $f'(\zeta_j)$ becomes more complicated if $f'(x)$ is a polynomial of an order higher than one. For example, if $f'(x) = a_0 + a_1 x + a_2 x^2 + a_3 x^3$,

$$\tau_j' = v\sqrt{2\pi} f'(\zeta_j) + v^3 \sqrt{2\pi} (3a_3 \zeta_j + a_2),$$

and it is difficult to evaluate the relevance of the two terms on the right-hand side until actual values for the parameters $v$ and $a_k$ are put in. Simulations have shown that when $\mathbf{t}$ is a good approximation of the true size distribution, the distances $d_\tau$ and $d_n$ attain values very close to each other; this is an *a posteriori* confirmation of the wisdom of approximating the kernels by normal distributions. During simulations in which a positive definite solution $\mathbf{f}'$ can be found for some value of $\gamma$, it happens that the value of $\gamma$ which produces a distance minimum may give rise to nonphysical situations since some of the components of $\mathbf{f}'$ are negative. The distance definition given in Eq. (10) eliminates to a large extent such a nuisance and allows an easy comprehension in cases in which it is still present. Other distance definitions, as, for example,

$$d = \frac{\|\mathbf{A}\mathbf{f}' - \boldsymbol{\tau}\|}{N\|\boldsymbol{\tau}\|} = \frac{\sum_1^N {}_j [(\mathbf{A}\mathbf{f}')_j - \tau_j]^2}{N \cdot \sum_1^N {}_j \tau_j^2} ,$$

often gave rise in our computations to the feature described above especially when the wavelength range in which the simulated optical depths were computed was from 0.3 to 1.6 $\mu$m or smaller.

The particular choice of distance $d_\tau$ and $d_n$ which has been made implies that the method is particularly sensitive to underestimations of the true solution by the retrieved one in the large particle region (LPR), a particle greater than $\sim$2 $\mu$m, and to overestimations in the small particle region (SPR), particles with radii less than $\sim$0.5 $\mu$m. It is a little sensitive to underestimations in the SPR, the major weakness of the choice.

When the true solution $n(x)$ is either a Junge- or a Deirmendjian-type the retrievals are somewhat trivial. In fact the initialization procedure (IP) gives rise to optical depths whose distance from the simulated depths is smaller than the most likely percentage error in actual measurements; moreover the retrieval technique applied to $\mathbf{t}$ produces the best solution for very high values of $\gamma$, that is, $\mathbf{f}'$ is very smooth.

Examples of such trivial retrievals are plotted in Figs. 3 and 4. All the relevant parameters $[n(x),\mathbf{t},x_I,x_F,\gamma_L]$, where $\gamma_L = \log\gamma$, are defined either in the figure or in the captions for easy reference. Figure 3 plots the distance $d_n$ vs $\gamma$ on a log–log scale. The best solution is achieved for a $\gamma_L = 0$ which is actually the maximum value allowed. For $\gamma_L$ less than $-1.39$ the retrieved solution $\mathbf{n}'$ is nonphysical since some values of $\mathbf{f}'$ are negative. However the transition between the nonphysical to well-behaved solutions is smooth in the sense that, starting from values of $\gamma_L$ such that the number of negative components or $\mathbf{f}'$ is three to four, (1) the negative $\mathbf{f}'$ components lie only in the SPR; (2) the retrieved values $\mathbf{f}'$ (and $\mathbf{n}'$) in that region increase monotonically with increasing $\gamma$ until a well-behaved solution is reached ($\gamma_L = -1.35$).

This feature is evident in the whole set of retrievals that have been made. When a positive solution is attainable from a certain $\mathbf{t}$, there is a value of $\gamma$ starting from which the solutions behave as described above. In most retrievals the first well-behaved solution is not the best one. When $\mathbf{t}$ is a Junge-type distribution [$n(x)$ being still a haze $M$] the retrieved best solution has two negative components ($\gamma_L = -1.85$), see Figs. 5 and 6. The solution is good in the LPR and no wavy structure is present in the solution. Distance $d_n$ is at its minimum because the LPR has a large weight in the computation of the distance itself. As the value of $\gamma$ increases the solution in the LPR worsens while the overall solution becomes well-behaved.

A best physical solution could be the one computed with $\gamma_L = 1.0$; however, another choice would be to adopt the best solution [the one whose distance $d_n$ from the $n(x)$ is lowest] and filter out the negative components; for the case shown in Fig. 6 one would obtain an extremely good inversion for radii ranging from 0.195 to 5 $\mu$m. It should be noted that the radius range can be increased to 10 $\mu$m and the $\mathbf{n}'$ obtained has the same quality as the one shown in Fig. 6.

Several problems arise if the radius range is extended in the SPR. No well-behaved solution in the radius range from 0.05 to 5 $\mu$m is attained for $10^{-7} \le \gamma \le 10^0$. The value $\gamma_L = -1.0$ is already too large to allow a good reconstruction of the LPR, which could be done for smaller values of $\gamma$ at the expense of missing completely

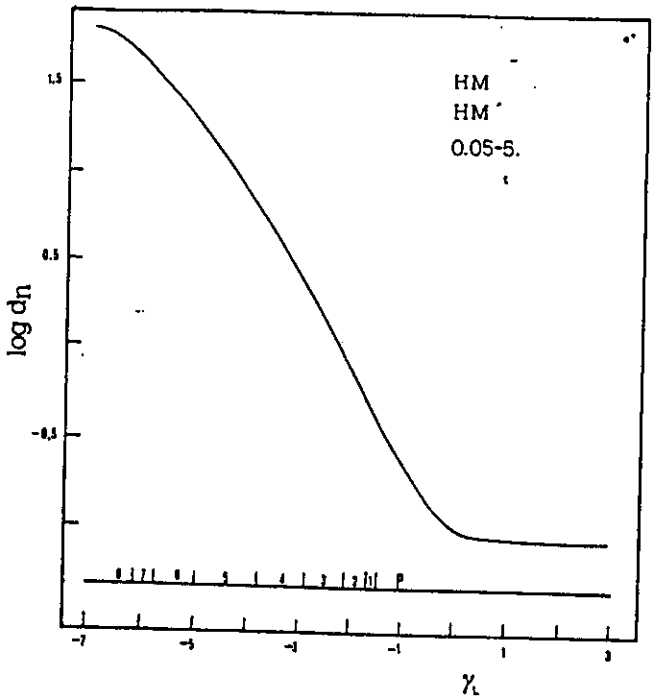


Fig. 3. Distance between retrieved and true size distribution $d_n$ vs $\gamma_L = \log\gamma$. The symbols in the upper right-hand corner refer to, from the highest to the lowest, true size distribution $n(x)$; first-guess solution t; and radius range (in microns) for t, f′ and n′. The numbers in the lower part of the figure represent the number of negative components in the retrieved f′ at a given $\gamma_L$; $P$ indicates the range of positive definite f′.

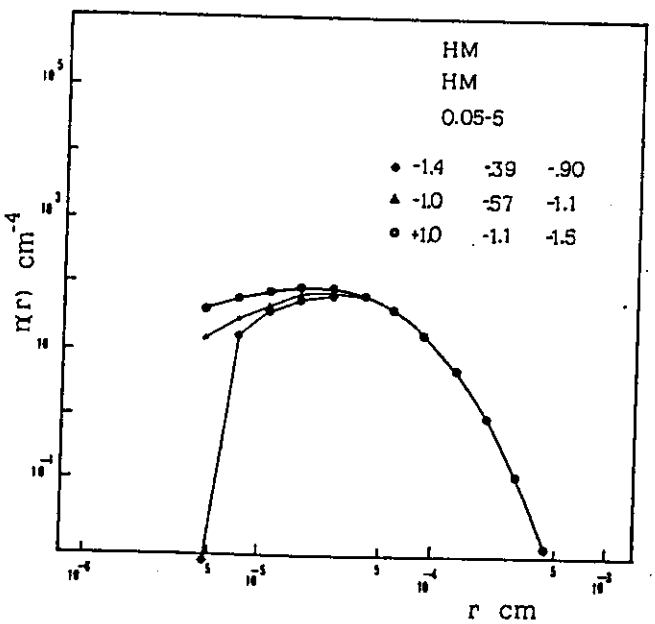


Fig. 4. Retrieved size distributions n′ (segments with symbols) and true size distribution $n(x)$ (solid line). The upper symbols in the right-hand corner are the same as shown in Fig. 3. The lower symbols denote, respectively (moving horizontally), the curve definition symbol; $\gamma_L = \log\gamma$ at which retrieval is done; $d_n$ (the distance between retrieved and true distributions); and $d_\tau$ (the distance between retrieved and true optical depths). Negative components when present are drawn below the abscissa scale.

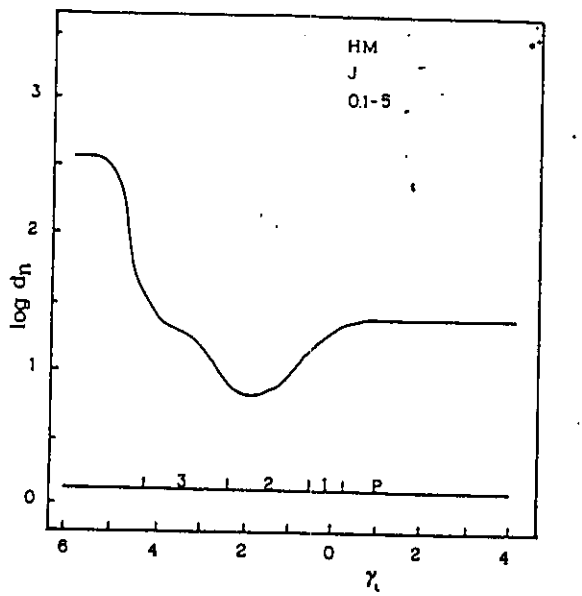


Fig. 5. Same as Fig. 3.

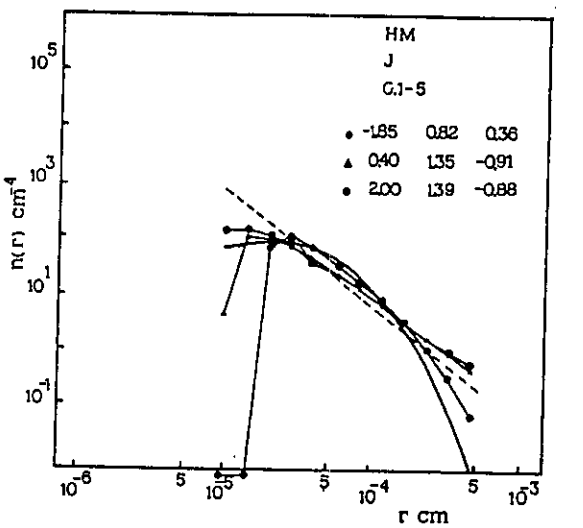


Fig. 6. Same as Fig. 4.

the information on the SPR. The change in shape of the solution in the SPR, as $\gamma$ increases, follows the pattern already described.

The ability of the retrieval method to cope with actual physical situations can be better discerned in Figs. 7 and 8. The true solution $n(x)$ is the $D3$ size distribution shown in Fig. 1. Figure 7 shows that a distance minimum is attained for a positive definite f′. The presence of the second mode produces a wavy structure ($\gamma_L = -3.6$) which is, however, smoothed out as $\gamma$ increases. The best solution ($\gamma_L = -2.25$) closely follows the structure of $n(x)$ for the middle range, and an honorable compromise is obtained in the rest of the radius range. Therefore, contrary to what happens when $n(x)$ is a haze $M$, well-behaved solutions are found in the radius range from 0.05 to 5 $\mu$m. A qualitative discussion of this behavior was given in Sec. III. The solution for a smaller range (0.1–5.0 $\mu$m) is not significantly different

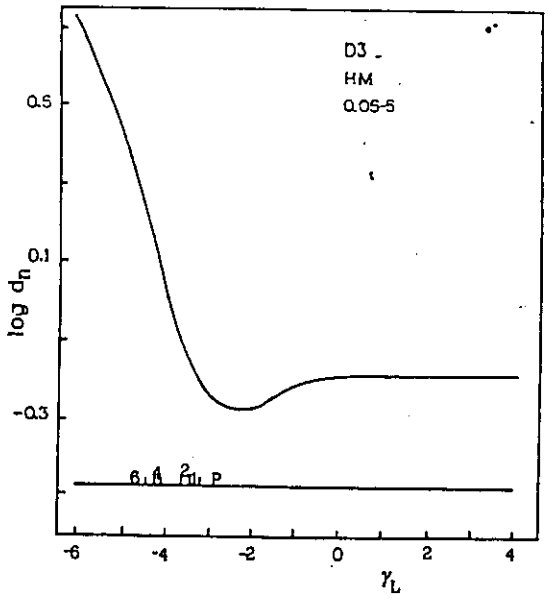


Fig. 7. Same as Fig. 3.

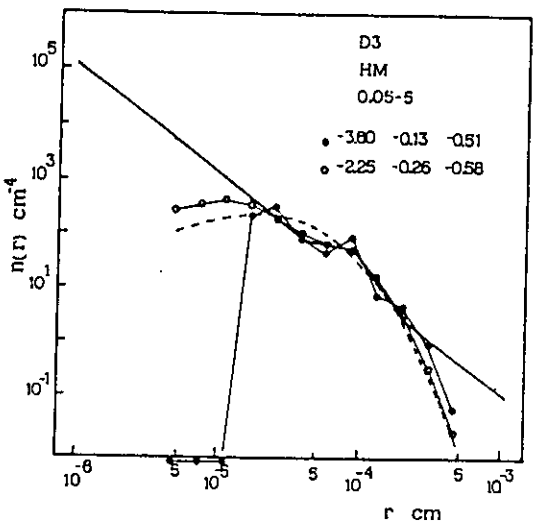


Fig. 8. Same as Fig. 4.

from that shown in Fig. 8.

The sensitivity of the adopted retrieval technique to the information content of simulated optical data can be seen when a $D4$ size distribution (shown in Fig. 1) is used as $n(x)$. The independent pieces of information, assuming a 5–10% experimental error, are slightly lower when compared with those contained in other sets of optical depths referred to in this paper. However, the ability of the linear method to retrieve such a size distribution is much lower than for the cases discussed up to now. In the whole set of inversions made no well-behaved solution has been found, negative components of f′ always being present in the SPR for $10^{-7} \leq \gamma \leq 1$. From Fig. 9 it is evident that, because of the relatively high value of $\gamma$ used in the computation, n′ retains much information on the structure of t′.

To inquire into the dependence of f′ on t some retrievals have been made using various t, the true solution again being a $D3$ size distribution. No well-behaved solution is obtained using a Junge or haze $L$ as t for $10^{-6} \leq \gamma \leq 1$, while solutions are found using haze $M$ (already shown in Fig. 8) and haze $H$ distributions. Figure 10 shows the distances $d_n$, while the actual retrieved size distributions are shown in Fig. 11. The $\gamma$ used in the computations are those for which a minimum distance $d_n$ is attained. While a well-behaved solution can be obtained with a haze $M$ as t from a certain $\gamma$ on, only a restricted range of $\gamma$ can be selected that produces well-behaved solutions when haze $H$ is chosen.

It is difficult to say whether the distance between the two solutions shown in Figs. 10 and 11 is large; it depends also on which $\gamma$ is selected for the inversion. Dealing with measured data there is no possibility of an automatic choice of the best $\gamma$. Moreover it has been pointed out that the solution may not be well-behaved but still be a good solution for some radius range. When

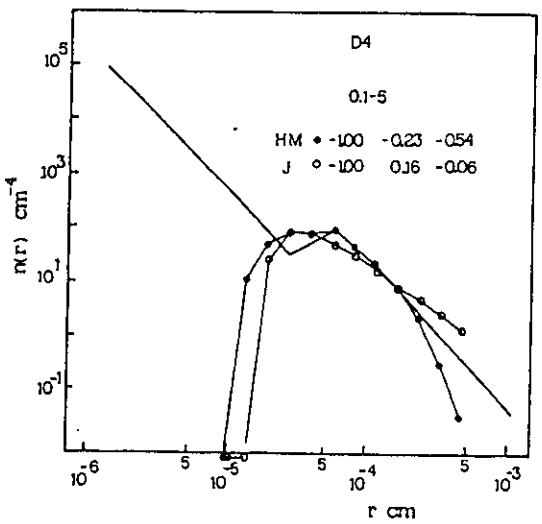


Fig. 9. Same as Fig. 4. The first trial solutions are defined to the left of the symbols.

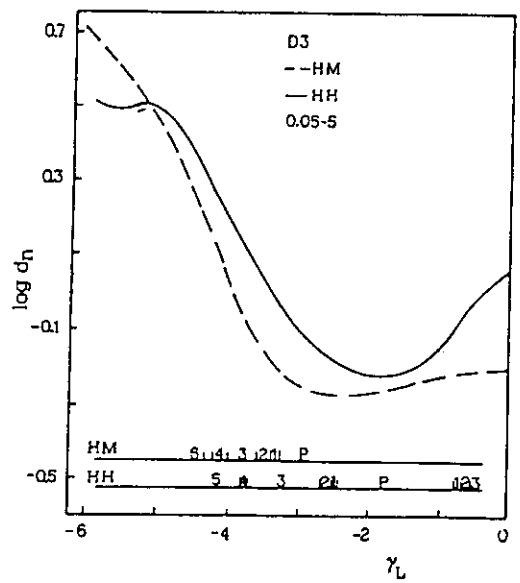


Fig. 10. Same as Fig. 3.

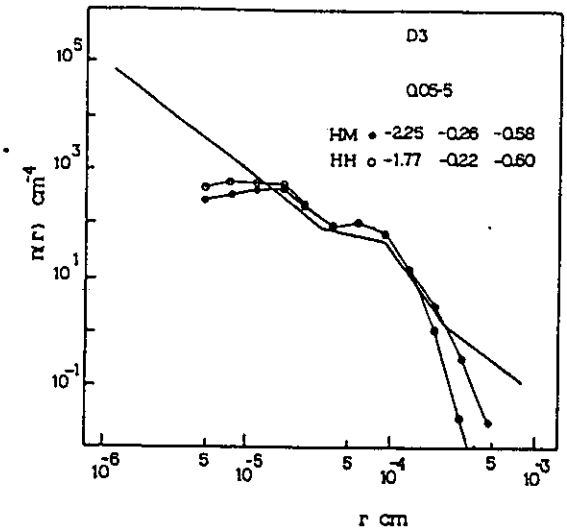


Fig. 11. Same as Fig. 9.

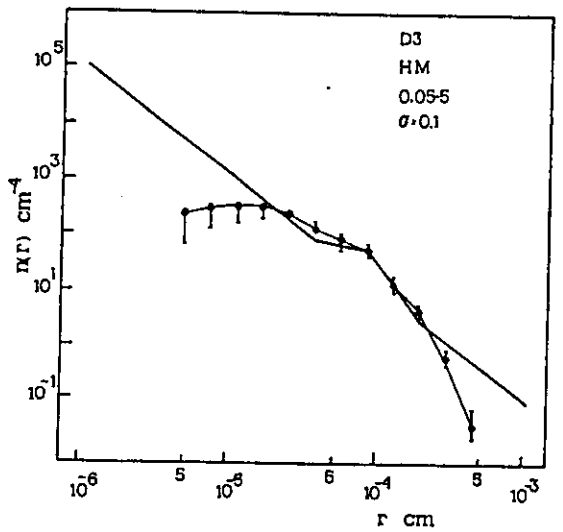


Fig. 12. Full explanation in the text.

the Junge distribution is selected as t, for example, n′ is extremely good in the middle and large particle range. Indeed when a well-behaved solution is obtained only for large values of $\gamma$ (say, $\gamma > 10^{-2}$), much information on the structure of t is retained on the n′. Therefore, when dealing with measured data, it may not be convenient to search only and exclusively for a well-behaved solution.

### D. Simulated Measurements with Added Random Errors

To investigate the effect of the superposition of random errors on the simulated optical depths it is necessary to perform computations with several sets of errors. The sensitivity of the retrieval techniques to these errors can be understood only by comparing the results of the whole set of inversions obtained.

Normally distributed random errors are used, of variance 0.05 and 0.1, simulating a 5–10% experimental error, which is the most likely percentage error range to be expected in actual extinction measurements over the wavelength range used in the computations. In case this range is extended into the infrared, for example, using simulated optical depths computed in the 8–13-$\mu$m atmospheric window, the quoted errors are no longer realistic since the percentage error in the latter wavelength range is likely to be ~30–40%. It is doubtful whether the inclusion of these wavelengths would increase the overall information content of the extinction data set.

The computations shown assume a $D3$ distribution as $n(x)$ and using a t of the haze $M$ type. For each of the 100 sets of errors (in each run the error is computed individually at each wavelength), the distance $d_n$ is computed for $10^{-6} \leq \gamma \leq 1$ and the best $\gamma$ is chosen, which minimizes $d_n$. In all cases but two, the best $\gamma$ produces a well-behaved solution.

Figure 12 shows the results of the whole set of computations for $\sigma = 0.1$. The bars indicate minimum and maximum values of $n'(r_k)$ in the radius classes ($k$ = 1,12) used in the computation; the asterisks indicate the arithmetic mean value $\bar{n}'(r_k)$. In Fig. 13 the distribution of values of $n_i(r_k)$ is plotted ($i$ = 1,100 is the run indicator) and for the radius ranges in which the dispersion is largest. The number of channels in each histogram is 90 (not all of them are shown); it coincides with the channel subdivision used in the ordinate axis of the figures in which the size distributions are shown. In every radius range the whole set of solutions shows a well-defined maximum. Deviations from the mean are greater in the SPR since the variability of the solution to small variations in $\gamma$ is larger in such a radius range. The inclusion of 10% random error does not

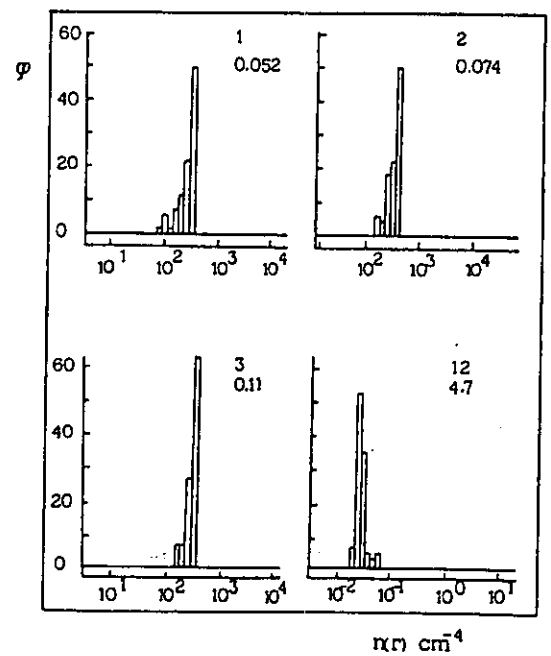


Fig. 13. Frequency distribution $\varphi$ of the number of particles $n_i(r_k)$ in a given radius class. The numbers in the upper right-hand corner of each subfigure denote the sequence and the numerical value (in microns) of the radius class under examination.

substantially modify the behavior in the SPR and LPR. There is a degradation of the information on the MPR which is smoothed out.

The pattern of retrieved distributions when 5% random errors are added ($\sigma$ = 0.05) is shown in Fig. 14. The most noticeable difference is the better agreement between $n(x)$ and $\mathbf{n}'$ in the MPR. Moreover the histograms of $n_i(r_k)$ (not shown) are narrower than those shown in Fig. 13.

## V. Concluding Remarks

Knowledge of aerosol properties is insufficient over a large portion of the globe. At the most, mean values are available but very little is known of the seasonal variations or smaller time scale and spatial fluctuations. It appears that only ground-based optical radiometric methods allow (1) a long-term monitoring of some of the aerosol properties (especially in the troposphere) because of the possibility of defining automatic data handling procedures, and (2) a sufficiently dense network because of the low cost of the instrumentation.

Our study deals with (simulated) atmospheric extinction measurements at the ground done in narrow spectral intervals. Any successful inversion technique applied to a given set of extinction optical depths produces a size distribution which is optically equivalent (in the wavelength range in which the optical depths are defined) to the true aerosol stratification in the atmosphere. Such an equivalent size distribution contains no information on actual size distributions to be found in specific layers in the atmosphere. Were the measurements carried out at the ground and, at the same time, also at various levels in the atmosphere, then, using the same inversion technique, the height variation of the size distribution could be computed from the extinction data set. However the equivalent size distribution can be used directly to compute the spectral direct solar irradiance reaching the ground; also, using suitable approximations of the transfer equation for turbid media, for example, Sobolev's,[19] it is possible to compute the distribution of solar spectral diffuse irradiance reaching the surface of the earth. To the extent that specific technical choices are inserted into the inversion algorithm to optimize the retrieval of the medium and large aerosol particles, the retrieved equivalent size distribution can be used to improve the computation of the aerosol contribution to the heat budget of the whole atmosphere.

In this paper a linear method is used to retrieve aerosol size distribution from spectral extinction data. It is a linear constrained method developed on the definition of distance between simulated and retrieved optical depths given in Eq. (8). The retrieval algorithm applied to a given first-guess solution may (or may not) produce well-behaved solutions, that is, a positive definite aerosol size distribution. However, the transition between nonphysical to well-behaved solutions, which is driven by the smoothing parameter $\gamma$, is gradual and the negative components, when present, always belong to the small particle range. Best solutions are found for $\gamma$ ranging from $10^{-4}$ to 0.05. In such conditions much

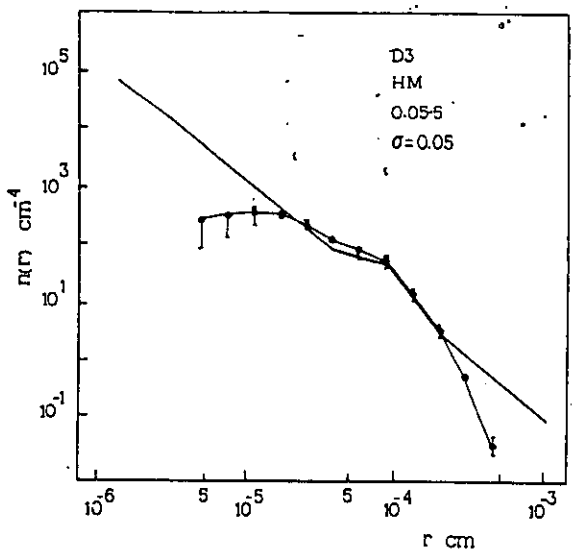


Fig. 14. Same as Fig. 12.

information on the shape of the true solution in the medium and large particle range is retained even if the retrieved distribution is not well-behaved in the small particle range. When higher values of $\gamma$ are required to obtain well-behaved solutions, usually a strong bias on the retrieved solution is posed by the form of the first-guess solution.

An estimate of the capability of the technique to retrieve optical data is obtained by adding normally distributed random errors to the optical depths, the variance of the percentage errors $\sigma$ being 0.1 and 0.05. The presence of errors degrades to some extent the ability of the technique to recover microphysical information of the size distribution. Practically, a radiometer measuring spectral extinction data, in the wavelength region from 0.35 to 2 $\mu$m, to be processed using inversion algorithms should allow the computation of aerosol optical depths with a rms error near 5%. No great reliability should be given to the retrieved distributions when this limit is severely exceeded.

R. Rizzi wishes to acknowledge the useful discussions with Franco Mattioli which led to untangling some of the intricacies of the mathematics of these inverse problems. R. Guzzi is now on leave at GNSM Istituto di Fisica, Ferrara.

This research was sponsored by CNR.

## References

1. E. P. Shettle and R. W. Fenn, "Models for the Aerosol of the Lower Atmosphere and the Effects of Humidity Variations on their Optical Properties," Technical Report AFGL-TR-79-0214 (AFGL, Bedford, Mass., 1979).
2. I. H. Blifford, Jr., and L. D. Ringer, J. Atmos. Sci. 26, 716 (1969).
3. D. J. Hofmann, J. M. Rosen, T. J. Pepin, and R. G. Pinnick, J. Atmos. Sci. 32, 1446 (1975).
4. J. M. Rosen, D. J. Hofmann, and J. Laby, J. Atmos. Sci. 32, 1457 (1975).

5. T. S. Cress, "Airborne Measurement of Aerosol Size Distributions over Northern Europe," Vol. 1, Spring and Fall-1976, Summer 1977. AFGL-TR-80-0178 (AFGL, Bedford, Mass., 1980).
6. M. D. King, D. M. Byrne, B. M. Herman, and J. A. Reagan, J. Atmos. Sci. 35, 2153 (1978).
7. C. Tomasi and R. Guzzi, J. Phys E 7, 647 (1974).
8. J. V. Dave, "Subroutines for Computing the Parameters of the Electromagnetic Radiation Scattered by a Sphere," IBM Report 320-3237 (IBM Scientific Center, Palo Alto, Calif., 1968).
9. L. Elterman, "UV, Visible and IR Attenuation for Altitudes to 50 km," Technical Report AFCRL-68-0153 (AFCRL, Bedford, Mass., 1968).
10. J. B. Gillespie, S. G. Jennings, and J. D. Lindberg, Appl. Opt. 17, 989 (1978).
11. S. Twomey, *Introduction to the Mathematics of Inversion in Remote Sensing and Indirect Measurements* (Elsevier, Amsterdam, 1977).
12. C. E. Junge, E. Robinson, and F. L. Ludwig, J. Appl. Meteorol. 8, 340 (1969).
13. D. Deirmendjian, *Electromagnetic Scattering on Spherical Polydispersion* (American Elsevier, New York, 1969).
14. B. L. Phillips, J. Assoc. Comput. Mach. 9, 84 (1962).
15. S. Twomey, J. Assoc. Comput. Mach. 10, 97 (1963).
16. S. Twomey, J. Franklin Inst. 279, 95 (1965).
17. G. Yamamoto and M. Tanaka, Appl. Opt. 8, 447 (1969).
18. G. E. Shaw, Appl. Opt. 18, 988 (1979).
19. V. V. Sobolev, *Light Scattering in Planetary Atmospheres* (Pergamon, New York, 1975).